Heliyon 10 (2024) e37443

Contents lists available at ScienceDirect

Heliyon

journal homepage: www.cell.com/heliyon

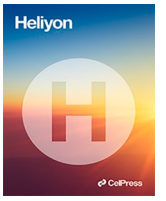

Research article

Thermal buckling analysis of reinforced composite conical shells in acidic environments: Numerical and experimental investigation on the effects of nanoparticles

Seyed Masoud Montazeri [a], Saeed Saber-Samandari [b,c,*], Seyed Ali Sadough Vanini [a]

[a] Department of Mechanical Engineering, Amirkabir University of Technology (Tehran Polytechnic), Tehran, Iran
[b] New Technologies Research Center (NTRC), Amirkabir University of Technology, Tehran, Iran
[c] Composites Research Laboratory (CRLab), Amirkabir University of Technology, Tehran, Iran

ARTICLE INFO

Keywords:
Composite shell
Hygrothermal buckling
Nanoparticles
Acid exposure

ABSTRACT

This study investigates the effects of acid penetration and temperature on the buckling behavior of conical composite shells, to enhance structural integrity and longevity in corrosive environments. The study explores the impact of acid exposure on thermal properties and examines the efficacy of incorporating nano-silica and nano-clay in preventing buckling. Additionally, it analyzes the influence of nanoparticles on the thermal, moisture, and mechanical properties of the composite material. Experimental assessments are conducted to measure material properties during exposure to a sulfuric acid solution, providing a comprehensive understanding of the material's behavior under extreme conditions. However, due to the complexity of investigating the combined effects of temperature, acid, and nanoparticles on composite shell buckling, a combined numerical and experimental approach is adopted to predict the critical buckling load. To this end, equations of conical shells under hygrothermal loading are derived, and the critical buckling load is determined through pre-buckling analysis. The Generalized Differential Quadrature (GDQ) method is employed to solve the hygrothermal buckling of the composite shell using experimentally obtained material properties. Comparative results are presented for different nanoparticles, shell geometries, and exposure times in acidic environments. The experiments reveal that adding nanoparticles enhances mechanical properties and reduces thermal and moisture expansion coefficients. Conversely, the acidic conditions deteriorate these properties. Numerical analysis demonstrates that incorporating nanoparticles significantly increases the critical buckling temperature, with nano-silica and nano-clay particles resulting in an 11.5 % and 34.2 % increase, respectively. However, acidic environments decrease the critical buckling temperature, with reductions of 32 % for unreinforced, 29 % for nano-silica reinforced, and 46 % for nano-clay reinforced composites after three months of exposure.

* Corresponding author. New Technologies Research Center (NTRC), Amirkabir University of Technology, Tehran, Iran.
E-mail address: saeedss@aut.ac.ir (S. Saber-Samandari).

https://doi.org/10.1016/j.heliyon.2024.e37443
Received 11 February 2024; Received in revised form 2 July 2024; Accepted 4 September 2024
Available online 6 September 2024

1. Introduction

Conical and cylindrical composite shells made of glass/epoxy are extensively utilized across aerospace, marine, and automotive industries. These shells often encounter harsh conditions, including corrosion, humidity, and elevated temperatures. Exposure to such environments can have detrimental effects on the mechanical and hygrothermal properties of these composite structures [1]. Additionally, the combination of humidity and temperature can induce internal loading within the structures, directly influencing their buckling behavior [2]. Acidic environments have direct or indirect effects on vibrations [3,4], impact response [5], and fatigue behavior [6]. Studies have shown that exposure to corrosive and humid environments leads to a significant decline in GFRP's mechanical properties [7–9]. Corrosive environments cause complex degradation in composites through chemical and physical mechanisms. Moisture absorption contributes to fiber/matrix interface failure and matrix embrittlement, decreasing strength, stiffness, and dimensional stability [10,11]. Furthermore, moisture can negatively affect the bonding between the fiber and matrix, resulting in a weak interface, differential swelling, and matrix fractures [12].

Extensive research has been conducted on the mechanical [13–15], thermal [16,17], and moisture-induced buckling [18] of cylindrical and conical shells under a variety of conditions and with different materials [19–26]. Furthermore, various studies have reported that corrosive conditions can adversely affect the buckling behavior of composite structures due to acid penetration at the matrix-fiber interface [27,28]. Samir Emam and Eltaher [29] investigated the buckling and post-buckling behavior of a composite beam under hygrothermal conditions. Biswal et al. [30] explored the numerical and experimental free vibration behavior of woven Glass/Epoxy laminated composite shells under hygrothermal conditions. The findings revealed that as temperature and moisture increase, the natural frequency of the laminated composite shells decreases. Song et al. [31] investigated the vibration of laminated composite conical shells under hygrothermal conditions and arbitrary supports. The influence of a thermal and humid environment and boundary stiffness on the vibration was studied through theoretical analysis, experiments, and finite element methods.

In another study by Biswal et al. [32] investigated the impact of various temperature and humidity conditions on the buckling behavior of composite cylindrical shell panels. The results demonstrated a decrease in critical load buckling with increasing temperature and humidity concentration, attributed to reduced stiffness. Heidari-Soureshjani et al. [33] analyzed the buckling and vibration of joined functionally graded porous (FGP) conical-conical shells under hygro-thermal environments, focusing on different porosity distributions and their effects on frequency trends from room conditions to hygro-thermal buckling states.

In recent years, the incorporation of nanoparticles has revolutionized the manipulation of mechanical and hygrothermal characteristics of composite materials [34–36]. Nanoparticles have been shown to be significantly effective in reducing the composite material's thermal expansion due to their lower coefficient of thermal expansion [37,38]. Numerous investigations have indicated that incorporating silica and clay nanoparticles into the matrix of composites enhances mechanical [39,40] and thermal [41,42] properties. Additionally, nanoparticles have been shown to mitigate the deterioration of mechanical properties induced by corrosive environments. Vishnu et al. [43] observed that vinyl ester/glass properties were compromised by moisture absorption time in alkaline solutions. However, nano-clay samples demonstrated superior retention of mechanical properties compared to the pristine sample owing to reduced moisture absorption. Gitiara et al. [44] explored the low-impact properties of GFRP with varying percentages of nano-clay and nano-silica in sulfuric acid. The study revealed that while immersion time resulted in decreased mechanical properties, adding nanoparticles improved these properties, and nano-clay samples exhibited lower moisture absorption levels compared to pure and nano-silica samples.

Nanoparticles can also be remarkably effective in improving the buckling resistance of composite structures. Rafiee et al. [45] conducted an experimental study on the buckling of graphene/epoxy nanocomposite beams and reported a substantial rise in the critical buckling load by incorporating 0.1%wt. graphene platelets into the epoxy matrix. Ozkan Ozbek [46] performed experimental analysis to examine the influence of nano-silica on the buckling behavior of composite sheets reinforced with kevlar/epoxy fibers at varying weight percentages. The study revealed that the addition of nanoparticles significantly elevated the buckling load. Bozkurt et al. [47] carried out an experimental investigation into buckling by evaluating the mechanical properties of S-glass/epoxy composites reinforced with fibers containing nano-clay using tensile and bending tests. Their findings demonstrated that incorporating 1 % by weight of nano-clay into the composite samples enhanced the buckling load by 8 %.

Numerous numerical methods exist for solving the governing equations of shells and plates, each with distinct advantages tailored to specific problem characteristics and accuracy requirements. In this research, the Generalized Differential Quadrature (GDQ) method is chosen due to its effectiveness in predicting critical buckling loads for composite structures. GDQ expands upon the Differential Quadrature (DQ) method by utilizing generalized polynomial approximations to discretize partial differential equations into algebraic forms. A significant advantage of GDQ over traditional DQ methods is its improved capability to handle irregular and non-uniform grid distributions more efficiently, thereby enhancing solution accuracy without a substantial increase in computational costs [48,49]. Qingyang Huang et al. [50] utilized GDQ for free vibration analysis of carbon fiber/epoxy resin and carbon/carbon plain woven conical-cylindrical shells under thermal environments with general boundary conditions. Qingquan You et al. [51] employed GDQ for buckling analysis of functionally graded carbon nanotube reinforced composite (FG-CNTRC) joined conical–cylindrical laminated shells, considering thermal effects and achieving significant reduction in computational time compared to FEM.

Studying the acidic environments' effects on hygrothermal buckling in conical and cylindrical composite structures is important. However, relatively few studies have investigated the hygrothermal buckling analysis of nanoparticle-reinforced glass/epoxy composite structures based on experimentally obtained material properties. Additionally, to the author's knowledge, no work has been done to assess the influence of sulfuric acid solutions on the thermal properties and thermal buckling of composite structures.

This research combines numerical and experimental procedures to study the hygrothermal buckling behavior of conical and cylindrical shells and investigates the influence of nanoparticles in glass/epoxy composites. To experimentally determine the mechanical

properties and thermal and moisture expansion coefficients of the composite material, epoxy/glass samples reinforced with nano-silica and nano-clay were fabricated. The samples were exposed to sulfuric acid for different periods, and their mechanical and thermal properties (E, ν, G, α, Tg) were measured and analyzed. Moreover, the coefficient of moisture expansion in sulfuric acid was calculated for the composite samples. The governing equations associated with the buckling of conical and cylindrical shells were acquired based on the first-order shear deformation theory (FSDT). Additionally, pre-buckling analysis was conducted, and the governing equations were solved utilizing the GDQ technique. The mechanical, thermal, and moisture properties were incorporated into the governing equations to determine the critical buckling temperature of conical and cylindrical shells. The effects of nanoparticles, corrosive environment, hygric loads, shell geometry, and boundary conditions were examined and presented.

This study provides novel insights by integrating experimental data with numerical methods to comprehensively analyze the hygrothermal buckling behavior of composite structures in acidic environments. It includes an assessment of the effects of sulfuric acid solutions on the thermal properties and thermal buckling of these structures, which has not been extensively explored previously.

2. Experimentation

2.1. Materials

To fabricate nanoparticle-reinforced specimens, epoxy resin EPON 828 and DETA hardener were blended with woven C-glass fibers. C-glass weave fabric delivers significant benefits at the macro level, including substantial strength in two in-plane directions and reduced weight [52]. C-glass fabric is mostly utilized for chemical resistance applications in various studies [53]. Alongside woven C-glass fibers, organic plate-like nano-clay (montmorillonite 15A) and spherical nano-silica were employed as nanoscale reinforcements in the study. These nanoparticles are among the most frequently used in research work [3]. Adding nanoparticles not only improves the mechanical properties of composite materials but also reduces the moisture uptake and works as a barrier to acid penetration and deterioration by adding the tortuosity of the diffusion path [54]. Furthermore, the introduction of nanoparticles can reduce the coefficient of thermal expansion of composite materials due to their lower coefficient of thermal expansion compared to the polymeric matrix [55–57]. In fact, nanoparticles act as a mechanical constraint against thermal expansion. The extent of the reduction in the coefficient of thermal expansion is related to the rigidity of the particles and their suitable dispersion within the matrix [42].

2.2. Sample preparation

The properties of nanocomposites are heavily influenced by the proper dispersion of nanoparticles in the polymer matrix. Excessive amounts of nanoparticles and poor distribution can result in nanoparticle agglomeration, causing a substantial decline in mechanical properties [58]. Therefore, in this study, 3 % wt. of nanoparticles was utilized and a suitable fabrication process was carefully selected based on previous studies [59,60].

Initially, a mechanical mixer operating at 2000 rpm was employed for 30 min to distribute nanoparticles evenly within the epoxy resin. Subsequently, a sonication process was conducted to guarantee the uniform dispersion of nano-silica and nano-clay. To eliminate air bubbles formed during mixing, the mixture was placed in a vacuum oven for 20 min. Following that, a hardening agent was added in a 1:10 ratio and gently stirred with a metal wire to prevent further air entrapment. Six layers of woven glass fibers (300×300 mm^2) and two sheets of peel ply were laminated with a hand lay-up procedure. After 24 h, the polymer bonds were developed, and the resin was hardened. In the final stage of sample preparation, the nanocomposite sheets were precisely cut to standard dimensions using a water jet cutting technique. Additionally, some specimens were specifically cut at a 45-degree fiber angle to obtain their shear modulus. Subsequently, some of the samples underwent mechanical testing, while the remaining samples were subjected to acidic conditioning and then characterized by mechanical testing. To simulate an acidic environment, the samples were immersed in 5%wt. sulfuric acid for 1 and 3 months. During immersion, the pH of the acid was monitored and adjusted once per month to minimize the influence of fluctuating acid concentration.

2.3. Material characterization

2.3.1. Tensile testing

Young's modulus, shear modulus, and Poisson's ratio were obtained using tensile testing according to ASTM D3039 and D3518, using the STM-50 universal testing machine from SANTAM company. Herein, the loading speed was set to 2 mm/min. Three samples of each type underwent tensile testing, and the average value was employed in calculations. Since weave fabric was utilized, Young's modulus is assumed to be equal in two directions 1 and 2 and the shear modulus is considered the same in all directions based on previous studies [61]. Having said that, Eq. (1) was used to calculate the shear modulus of composite samples in which E_x was obtained from the aforementioned tensile test with 45° fiber direction [44].

$$G_{12} = \frac{1}{\frac{4}{E_x} - \frac{1}{E_{11}} - \frac{1}{E_{22}} + \frac{2\nu_{12}}{E_1}} \tag{1}$$

2.3.2. Coefficient of moisture expansion (CME)

The study of buckling in composite structures exposed to environmental conditions necessitates consideration of the expansion effects induced by moisture or other chemical solutions that permeate the material. These expansion effects can lead to internal forces

within the structure under certain boundary conditions. A critical component of this research is determining the coefficient of moisture expansion (CME) for nanoparticle-reinforced samples exposed to acidic solutions. While there is no standardized method for determining the CME of composites immersed in dilute sulfuric acid, the slope of the graph plotting strain against moisture uptake of samples immersed in acidic solutions can be used as a proxy for the expansion coefficient [62,63]. This approach enables the calculation of the CME as follows:

$$\beta = \frac{\frac{\Delta L}{L_i}}{\frac{\Delta M}{M_i}} \tag{2}$$

in Eq. (2), β is the coefficient of moisture expansion, L_i and M_i are the initial length and weight of the sample, and ΔL and ΔM are the variations of length and weight after the immersion period which represent the stain and moisture intake respectively. To enhance the precision of the experimental results and ensure consistency across samples, 20 specimens (25 × 25 mm) were cut from the original composite sheet using a water-jet process. The samples were drawn from three distinct groups: without nanoparticle reinforcement, 3%wt. nano-silica reinforcement, and 3%wt. nano-clay reinforcement. To eliminate any inherent moisture content, all samples were preheated in an oven at 50 °C for 4 h. Later, the samples were placed in sulfuric acid solution for three months. In this period, every three days, samples were taken out from acidic solution, wiped to dry the surface, monitored in terms of weight and length, and then immediately returned to the solution. The weight of samples was measured using a digital balance (0.001 g precision), and the length was obtained by a profile projector (0.001 mm precision). Finally, the slope of the graph acquired from the variation in length and weight was measured for all samples. The coefficient of moisture expansion for each composite sample in acidic environmental conditions was obtained by averaging these data.

2.3.3. Glass transition temperature

To evaluate the thermal response of nanocomposite samples and obtain their glass transition temperature, a differential scanning calorimetry (DSC) test was conducted following ASTM D7426-08 guidelines. Since a significant change in material behavior occurs at the glass transition temperature, it is a crucial parameter that demands consideration [64]. Therefore, in this study, buckling analysis was conducted below this temperature to guarantee that the material properties of the composite remain unaffected by temperature variations. Furthermore, to reliably measure the coefficient of thermal expansion, the dilatometer's temperature must be kept below the glass transition temperature.

2.3.4. Coefficient of thermal expansion (CTE)

The coefficient of thermal expansion (CTE) of polymers plays an important role in designing polymeric composite structures facing thermal environments. Therefore, investigating the impact of incorporating nanoparticles and subjecting the material to acidic conditions on its CTE is of paramount significance. This is a crucial objective of the present study. As defined by ASTM E 228–11, the coefficient of thermal expansion (CTE) of any solid material can be calculated by Eq. (3). It is determined by the slope between two points on the strain-temperature curve, representing the expansion of a specimen (from L_1 to L_2) within a specific temperature range (from T_1 to T_2) from its initial length of L_0 measured at a reference temperature T_0.

$$\alpha = \frac{\frac{L_2 - L_1}{L_0}}{T_2 - T_1} = \frac{1}{L_0}\frac{\Delta L}{\Delta T} \tag{3}$$

in Eq. (3), α is the coefficient of thermal expansion. To obtain this coefficient for nanoparticle-reinforced composite samples, they were cut in coupons with the size of 42 × 6x3 mm, and utilizing a dilatometer, the samples underwent a thermal loading in the temperature range of 25–200 °C with a heating rate of 5C/min. The slope of the strain-temperature graph was measured and presented as the coefficient of thermal expansion.

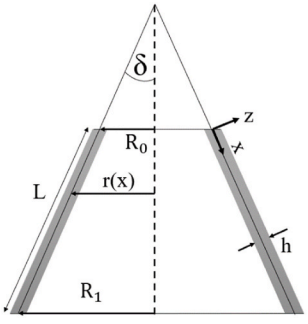

Fig. 1. Schematic presentation of conical shell geometry and coordinate system.

3. Theoretical formulation

3.1. Constitutive equations

According to Fig. 1, a conical shell is assumed with the length of L and thickness of h. The radius of the cone at any point in the longitudinal direction is defined as $r(x) = R_0 + xsin(\delta)$, in which R_0 is the smallest radius of the cone and δ is the semi-vertex angle of the cone. The thickness of the shell varies between -h/2 and +h/2. It is worth mentioning that setting the cone angle (δ) to zero generates a cylindrical shell.

First-order shear deformation theory (FSDT) was used to derive the governing equations for conical and cylindrical shells. According to FSDT, the displacement components in the shell can be expressed in terms of displacements and rotations of the reference middle surface ($z = 0$) as follows [65]:

$$\begin{aligned} u(x,\theta,z) &= u_0(x,\theta) + z\varphi_x(x,\theta) \\ v(x,\theta,z) &= v_0(x,\theta) + z\varphi_\theta(x,\theta) \\ w(x,\theta,z) &= w_0(x,\theta) \end{aligned} \tag{4}$$

in Eq. (4), u_0, v_0, and w_0 denote for the displacements of any point on the middle surface of the shell along the meridian, circumferential and thickness directions, respectively. Moreover, φ_x and φ_θ are transverse normal rotations around θ and x axes. The strain-displacement relations in the shell can be expressed as [66]:

$$\begin{Bmatrix} \varepsilon_{xx} \\ \varepsilon_{\theta\theta} \\ \gamma_{x\theta} \\ \gamma_{xz} \\ \gamma_{\theta z} \end{Bmatrix} = \begin{Bmatrix} \varepsilon^0_{xx} \\ \varepsilon^0_{\theta\theta} \\ \gamma^0_{x\theta} \\ \gamma^0_{xz} \\ \gamma^0_{xz} \end{Bmatrix} + z \begin{Bmatrix} k_{xx} \\ k_{\theta\theta} \\ k_{x\theta} \\ k_{xz} \\ k_{\theta z} \end{Bmatrix} \tag{5}$$

The strain components in terms of displacements can be written as follows [67]:

$$\begin{Bmatrix} \varepsilon^0_{xx} \\ \varepsilon^0_{\theta\theta} \\ \gamma^0_{x\theta} \\ \gamma^0_{xz} \\ \gamma^0_{xz} \end{Bmatrix} = \begin{Bmatrix} u_{0,x} \\ \frac{v_{0,\theta}}{r(x)} + \frac{\cos\delta}{r(x)} w_0 + \frac{\sin\delta}{r(x)} u_0 \\ \frac{u_{0,\theta}}{r(x)} + v_{0,x} - \frac{\sin\delta}{r(x)} v_0 \\ w_{0,x} + \varphi_x \\ \frac{w_{0,\theta}}{r(x)} - \frac{\cos\delta}{r(x)} v_0 + \varphi_x \end{Bmatrix} + \frac{1}{2} \begin{Bmatrix} w^2_{0,x} \\ \frac{1}{r^2(x)} w^2_{0,\theta} \\ \frac{2}{r(x)} w_{0,\theta} w_{0,x} \\ 0 \\ 0 \end{Bmatrix} \tag{6}$$

$$\begin{Bmatrix} k_{xx} \\ k_{\theta\theta} \\ k_{x\theta} \\ k_{xz} \\ k_{\theta z} \end{Bmatrix} = \begin{Bmatrix} \varphi_{x,x} \\ \frac{\varphi_{\theta,\theta}}{r(x)} + \frac{\sin\delta}{r(x)} \varphi_x \\ \frac{\varphi_{x,\theta}}{r(x)} + \varphi_{x,\theta} - \frac{\sin\delta}{r(x)} \varphi_\theta \\ 0 \\ 0 \end{Bmatrix} \tag{7}$$

in Eqs (5)–(7), the subscripts $,x$ and $,\theta$ are representative for the derivatives in x and θ directions, respectively. For a material with linear elastic behavior, the components of stress-strain equations regarding the hygrothermal loads can be defined as [67]:

$$\begin{Bmatrix} \sigma_{xx} \\ \sigma_{\theta\theta} \\ \sigma_{\theta z} \\ \sigma_{xz} \\ \sigma_{x\theta} \end{Bmatrix} = \begin{bmatrix} \overline{Q}_{11} & \overline{Q}_{12} & 0 & 0 & \overline{Q}_{16} \\ \overline{Q}_{12} & \overline{Q}_{22} & 0 & 0 & \overline{Q}_{26} \\ 0 & 0 & \overline{Q}_{44} & \overline{Q}_{45} & 0 \\ 0 & 0 & \overline{Q}_{45} & \overline{Q}_{55} & 0 \\ \overline{Q}_{16} & \overline{Q}_{26} & 0 & 0 & \overline{Q}_{66} \end{bmatrix} \begin{Bmatrix} \varepsilon_{xx} - \beta_{xx}\Delta C - \alpha_{xx}\Delta T \\ \varepsilon_{\theta\theta} - \beta_{\theta\theta}\Delta C - \alpha_{\theta\theta}\Delta T \\ \gamma_{\theta z} \\ \gamma_{xz} \\ \gamma_{x\theta} - 2\beta_{x\theta}\Delta C - 2\alpha_{x\theta}\Delta T \end{Bmatrix} \tag{8}$$

In Eq. (8) the coefficients $\overline{Q}_{11}, \overline{Q}_{12}, \overline{Q}_{22}, \overline{Q}_{44}, \overline{Q}_{55}$, and $\overline{Q}_{66}$ are called transformed reduced stiffness coefficients in plain stress condition. These coefficients are functions of $Q_{11}, Q_{12}, Q_{22}, Q_{44}, Q_{55}$, and Q_{66} , which represent reduced stiffness coefficients related to the principal directions of the composite. Their values are functions of $E_{11}, E_{22}, G_{12}, G_{13}, G_{23}$, and ν_{12}, calculated in this study based on experimental tests. Detailed calculations of these coefficients are provided in Ref. [68]. α_{xx} , $\alpha_{\theta\theta}$ and $\alpha_{x\theta}$ are the coefficients of thermal

expansion and β_{xx} , $\beta_{\theta\theta}$ and $\beta_{x\theta}$ are the coefficients of moisture expansion, which are introduced in Ref. [68].

Furthermore, ΔT is the temperature rise and ΔC is the amount of absorbed moisture in composite structure. Since Eq. (8) is applied to a single-layer composite, the coefficients A_{ij}, B_{ij}, and D_{ij} are employed to describe a laminated composite structure and are calculated as follows [68]:

$$\begin{aligned} A_{ij} &= \sum_{k=1}^{N} \overline{Q}_{ij}^{(k)} (Z_k - Z_{k-1}) \\ B_{ij} &= \frac{1}{2} \sum_{k=1}^{N} \overline{Q}_{ij}^{(k)} (Z_k^2 - Z_{k-1}^2) \\ D_{ij} &= \frac{1}{3} \sum_{k=1}^{N} \overline{Q}_{ij}^{(k)} (Z_k^3 - Z_{k-1}^3) \end{aligned} \tag{9}$$

where k represents the number of layers, N represents the number of composite layers, and Z_k represents the distance from the reference plane for each layer within the thickness direction. the force and moment resultants are determined by integrating the stress components across the thickness as presented in Eq. (10) [69]:

$$\begin{Bmatrix} N_{xx} \\ N_{\theta\theta} \\ N_{x\theta} \\ M_{xx} \\ M_{\theta\theta} \\ M_{x\theta} \\ Q_{\theta z} \\ Q_{xz} \end{Bmatrix} = \int_{-\frac{h}{2}}^{+\frac{h}{2}} \begin{Bmatrix} \sigma_{xx} \\ \sigma_{\theta\theta} \\ \sigma_{x\theta} \\ z\sigma_{xx} \\ z\sigma_{\theta\theta} \\ z\sigma_{x\theta} \\ k_s\sigma_{\theta z} \\ k_s\sigma_{xz} \end{Bmatrix} dz \tag{10}$$

The shear correction factor (k_s) is a crucial parameter in first-order shear theory. It is used to ensure that the strain energy generated by the transverse shear stresses ($Q_{\theta z}$ ، Q_{xz}) is equivalent to the strain energy produced by the actual transverse stresses predicted by three-dimensional elasticity theory. As a result, the shear correction factor (k_s) varies depending on various factors, including the material type, loading conditions, and boundary conditions. In the existing literature, the shear correction factor is commonly assumed to be either $5/6$ or $\pi^2/12$. In this study, a value of $5/6$ was adopted for k_s [67].

$$\begin{Bmatrix} N_{xx} \\ N_{\theta\theta} \\ N_{x\theta} \\ M_{xx} \\ M_{\theta\theta} \\ M_{x\theta} \\ Q_{\theta z} \\ Q_{xz} \end{Bmatrix} = \begin{bmatrix} A_{11} & A_{12} & 0 & B_{11} & B_{12} & 0 & 0 & 0 \\ A_{12} & A_{22} & 0 & B_{12} & B_{22} & 0 & 0 & 0 \\ 0 & 0 & A_{66} & 0 & 0 & B_{66} & 0 & 0 \\ B_{11} & B_{12} & 0 & D_{11} & D_{12} & 0 & 0 & 0 \\ B_{12} & B_{22} & 0 & D_{12} & D_{22} & 0 & 0 & 0 \\ 0 & 0 & B_{66} & 0 & 0 & D_{66} & 0 & 0 \\ 0 & 0 & 0 & 0 & 0 & 0 & k_sA_{44} & 0 \\ 0 & 0 & 0 & 0 & 0 & 0 & 0 & k_sA_{55} \end{bmatrix} \begin{Bmatrix} \varepsilon_{xx} \\ \varepsilon_{\theta\theta} \\ \gamma_{x\theta} \\ k_{xx} \\ k_{\theta\theta} \\ k_{x\theta} \\ \gamma_{\theta z} \\ \gamma_{xz} \end{Bmatrix} - \begin{Bmatrix} N_{xx}^{TC} \\ N_{\theta\theta}^{TC} \\ 0 \\ M_{xx}^{TC} \\ M_{\theta\theta}^{TC} \\ 0 \\ 0 \\ 0 \end{Bmatrix} \tag{11}$$

The force and moment resultants are written in terms of stain components in Eq. (11) in which N_{xx}^{TC} and $N_{\theta\theta}^{TC}$ are internal forces and M_{xx}^{TC} and $M_{\theta\theta}^{TC}$ are the internal moments caused by temperature and moisture variations in longitudinal and tangential directions and acquired by Eqs. (12) and (13).

$$\begin{aligned} \begin{bmatrix} N_{xx}^{TC} \\ N_{\theta\theta}^{TC} \end{bmatrix} &= \sum_{k=1}^{N} \begin{bmatrix} \overline{Q}_{11} & \overline{Q}_{12} \\ \overline{Q}_{21} & \overline{Q}_{22} \end{bmatrix}^{(k)} \begin{bmatrix} \beta_{xx} \\ \beta_{\theta\theta} \end{bmatrix}^{(k)} (Z_k - Z_{k-1})\, \Delta c^{(k)} \\ &+ \sum_{k=1}^{N} \begin{bmatrix} \overline{Q}_{11} & \overline{Q}_{12} \\ \overline{Q}_{21} & \overline{Q}_{22} \end{bmatrix}^{(k)} \begin{bmatrix} \alpha_{xx} \\ \alpha_{\theta\theta} \end{bmatrix}^{(k)} (Z_k - Z_{k-1})\, \Delta T^{(k)} \end{aligned} \tag{12}$$

$$\begin{bmatrix} M_{xx}^{TC} \\ M_{\theta\theta}^{TC} \end{bmatrix} = \sum_{k=1}^{N} \begin{bmatrix} \overline{Q}_{11} & \overline{Q}_{12} \\ \overline{Q}_{21} & \overline{Q}_{22} \end{bmatrix}^{(k)} \begin{bmatrix} \beta_{xx} \\ \beta_{\theta\theta} \end{bmatrix}^{(k)} \frac{(Z_k^2 - Z_{k-1}^2)}{2} \Delta c^{(k)} + \sum_{k=1}^{N} \begin{bmatrix} \overline{Q}_{11} & \overline{Q}_{12} \\ \overline{Q}_{21} & \overline{Q}_{22} \end{bmatrix}^{(k)} \begin{bmatrix} \alpha_{xx} \\ \alpha_{\theta\theta} \end{bmatrix}^{(k)} \frac{(Z_k^2 - Z_{k-1}^2)}{2} \Delta T^{(k)} \tag{13}$$

3.2. Equilibrium equations

It should be noted that in this study symmetrical layers are considered for the composite shell to derive the equilibrium equations and boundary conditions. The equilibrium equations of the conical shell are derived using Hamilton's principle and presented as Eq. (14) [70]:

$$\delta u=0: N_{xx,x}+\frac{N_{x\theta,\theta}}{r(x)}+\frac{sin(\delta)}{r(x)}(N_{xx}-N_{\theta\theta})=0 \tag{14.a}$$

$$\delta v=0: \frac{N_{\theta\theta,\theta}}{r(x)}+N_{x\theta,x}+2\frac{sin(\delta)}{r(x)}N_{x\theta}+\frac{cos(\delta)}{r(x)}Q_{\theta z}=0 \tag{14.b}$$

$$\delta w=0: Q_{xz,x}+\frac{Q_{\theta z,\theta}}{r(x)}+\frac{sin(\delta)}{r(x)}Q_{xz}-\frac{cos(\delta)}{r(x)}N_{\theta\theta}-\frac{1}{r(x)}\left(r(x)\,N_{xx}w_{0,x}+\,N_{x\theta}w_{0,\theta}\right)_{,x}-\frac{1}{r(x)}\left(r(x)\,N_{\theta\theta}w_{0,\theta}+\,N_{x\theta}w_{0,x}\right)_{,\theta}=0 \tag{14.c}$$

$$\delta\varphi_x=0: M_{xx,x}+\frac{M_{x\theta,\theta}}{r(x)}+\frac{sin(\delta)}{r(x)}(M_{xx}-M_{\theta\theta})-Q_{xz}=0 \tag{14.d}$$

$$\delta\varphi_y=0: M_{x\theta,x}+\frac{M_{\theta\theta,\theta}}{r(x)}+2\frac{sin(\delta)}{r(x)}M_{x\theta}-Q_{\theta z}=0 \tag{14.e}$$

3.3. Pre-buckling

In the bifurcation analysis of structures, it is essential to examine deformations prior to buckling. In the case of a conical shell exposed to hygrothermal conditions and constrained from longitudinal movement, hygrothermal loading is induced. Under symmetric deformations, the shell follows a pre-buckling equilibrium path. However, for specific moisture and temperature levels, asymmetric deformations occur, leading to the existence of two distinct equilibrium paths. This section aims to compute the moisture and temperature values. In this research, the loading condition of the shell is symmetric, resulting in symmetric pre-buckling variations. The assumption of a membrane shell is employed for pre-buckling deformations, and the equations describing these deformations are linear with respect to symmetric membrane pre-buckling deformations, with all moments and curvatures eliminated from the symmetric linear equations. Hence, Eq. (14.a) and (14.c) are the remaining equations, presented below [66,70,71]:

$$N_{xx,x}+\frac{sin(\delta)}{r(x)}(N_{xx}-N_{\theta\theta})=0-\frac{cos(\delta)}{r(x)}N_{\theta\theta}=0 \tag{15}$$

According to Eq. (15), it can be obtained that $N_{\theta\theta}=0$. By substituting $N_{\theta\theta}=0$ in Eq. (14.a) and solving the equation, N_{xx} is obtained as $N_{xx}=\frac{C_1}{r(x)}$. Regarding the assumption of symmetric layers in Eq. (11), the coefficients B_{ij} vanish, and N_{xx} and $N_{\theta\theta}$ are extracted from Eq. (11) as:

$$\begin{bmatrix}N_{xx}\\N_{\theta\theta}\end{bmatrix}=\begin{bmatrix}A_{11}&A_{12}\\A_{12}&A_{22}\end{bmatrix}\begin{bmatrix}u_{0,x}\\\frac{\cos(\delta)w_0}{r(x)}+\frac{\sin(\delta)u_0}{r(x)}\end{bmatrix}-\begin{bmatrix}N_{xx}^{TC}\\N_{\theta\theta}^{TC}\end{bmatrix} \tag{16}$$

By setting $N_{\theta\theta}=0$ and $N_{xx}=\frac{C_1}{r(x)}$ in Eq. (16), Eq. (17) is acquired in terms of displacements.

$$\left(A_{11}A_{22}-A_{12}^2\right)u_{0,x}=A_{22}\,N_{xx}^{TC}-A_{12}\,N_{\theta\theta}^{TC}+\frac{C_1A_{22}}{r(x)} \tag{17}$$

Solving Eq. (17) results in:

$$u(x)=\frac{1}{A_{11}A_{12}-A_{12}^2}\left(A_{22}N_{xx}^{TC}-A_{12}\,N_{\theta\theta}^{TC}+\frac{C_1A_{22}\,Ln(r(x))}{\sin(\delta)}\right)+C_2 \tag{18}$$

The two constants C_1 and C_2 are obtained by using the condition of immovable shell boundary along the longitudinal direction i.e. $u(0)=u(L)=0$. The coefficient C_1 is calculated as:

$$C_1=-\frac{L\sin(\delta)\left(A_{12}\,N_{\theta\theta}^{TC}-A_{22}N_{xx}^{TC}\right)}{A_{22}\,Ln\left(1+\frac{L\,\sin(\delta)}{R1}\right)} \tag{19}$$

Considering $N_{xx}=\frac{C_1}{r(x)}$, the axial pre-buckling force is calculated as:

$$N_{xx} = -\frac{L\sin(\delta)\left(A_{12}\,N_{\theta\theta}^{TC} - A_{22}N_{xx}^{TC}\right)}{r(x)\,A_{22}\,Ln\left(1+\frac{L\sin(\delta)}{R1}\right)} \tag{20}$$

3.4. Stability equations

A conical shell's stability equations can be expressed using the adjacent equilibrium criterion. Based on this criterion, the displacement field in a position adjacent to those in the pre-buckling state may be evaluated by adding a small perturbation to the pre-buckling state displacement. The introduced displacement components in Eq. (21), indicated by superscript 1, are nonzero but sufficiently small. As a result, the displacement field is considered in an adjacent equilibrium position, expressed as follows [70]:

$$\begin{Bmatrix} u_0(x,\theta) \\ v_0(x,\theta) \\ w_0(x,\theta) \\ \varphi_x(x,\theta) \\ \varphi_\theta(x,\theta) \end{Bmatrix} = \begin{Bmatrix} u_0^0(x) \\ v_0^0(x) \\ w_0^0(x) \\ \varphi_x^0(x) \\ \varphi_\theta^0(x) \end{Bmatrix} + \begin{Bmatrix} u_0^1(x,\theta) \\ v_0^1(x,\theta) \\ w_0^1(x,\theta) \\ \varphi_x^1(x,\theta) \\ \varphi_\theta^1(x,\theta) \end{Bmatrix} \tag{21}$$

By substituting Eq. (21) in (11), we can determine the incremental values of stress resultants. Since the incremental displacements are relatively small, the displacement components of the stress resultants can be approximated as linear. This allows us to obtain the stability equations by substituting these linearized stress resultants into the equilibrium equations and neglecting the pre-buckling equilibrium state [72]. The stability equations are summarized in Eq. (22).

$$N^1_{xx,x} + \frac{N^1_{x\theta,\theta}}{r(x)} + \frac{\sin(\delta)}{r(x)}\left(N^1_{xx} - N^1_{\theta\theta}\right) = 0 \tag{22.a}$$

$$\frac{N^1_{\theta\theta,\theta}}{r(x)} + N^1_{x\theta,\theta} + 2\frac{\sin(\delta)}{r(x)}N^1_{x\theta} + \frac{\cos(\delta)}{r(x)}Q^1_{\theta z} = 0 \tag{22.b}$$

$$Q^1_{xz,x} + \frac{Q^1_{\theta z,\theta}}{r(x)} + \frac{\sin(\delta)}{r(x)}Q^1_{xz} - \frac{\cos(\delta)}{r(x)}N^1_{\theta\theta} + \frac{L\sin(\delta)\left(A_{22}N_{xx}^{TC} - A_{12}\,N_{\theta\theta}^{TC}\right)}{r(x)\,A_{22}\,Ln\left(1+\frac{L\sin(\delta)}{R_0}\right)}\,w^1_{0,xx} = 0 \tag{22.c}$$

$$M^1_{xx,x} + \frac{M^1_{x\theta,\theta}}{r(x)} + \frac{\sin(\delta)}{r(x)}\left(M^1_{xx} - M^1_{\theta\theta}\right) - Q^1_{xz} = 0 \tag{22.d}$$

$$M^1_{x\theta,x} + \frac{M^1_{\theta\theta,\theta}}{r(x)} + 2\frac{\sin(\delta)}{r(x)}M^1_{x\theta} - Q^1_{\theta z} = 0 \tag{22.e}$$

By substituting Eq. (11) in Eq. (22) and using Eqs. (5)–(7), the governing equations of the composite conical shell are obtained and presented in the Appendix. Utilizing the separation of variables technique and Fourier series, the displacement components u_0, v_0 and w_0 and shear rotations φ_x and φ_θ can be expressed as follows [73]:

$$\begin{aligned} u_0(x,\theta) &= U(x)cos(n\theta) \\ v_0(x,\theta) &= V(x)sin(n\theta) \\ w_0(x,\theta) &= W(x)cos(n\theta) \\ \varphi_x(x,\theta) &= \Phi_x(x)cos(n\theta) \\ \varphi_\theta(x,\theta) &= \Phi_\theta(x)sin(n\theta) \end{aligned} \tag{23}$$

in Eq. (23), the integer n is the circumferential wave number of the corresponding mode shape. $U(x)$, (x) , $W(x)$, $\Phi_x(x)$, $\Phi_\theta(x)$ are unknown variables. By substituting Eq. (23) in Eqs. A1-A5 provided in the Appendix, multiplying the equations by cos θ or sin θ and integrating in the circumferential direction from 0 to 2π, Eq. (24) is obtained. This equation is expressed in terms of x variable, and independent of θ.

$$P_{111}U + P_{112}\frac{dU}{dx} + P_{113}\frac{d^2U}{dx^2} + P_{121}V + P_{122}\frac{dV}{dx} + P_{131}W + P_{132}\frac{dW}{dx} + P_{141}\Phi_x + P_{142}\frac{d\Phi_x}{dx} + P_{143}\frac{d^2\Phi_x}{dx^2} + P_{151}\Phi_\theta + P_{152}\frac{d\Phi_\theta}{dx} = 0 \tag{24.a}$$

$$P_{211}U + P_{212}\frac{dU}{dx} + P_{221}V + P_{222}\frac{dV}{dx} + P_{223}\frac{d^2V}{dx^2} + P_{231}W + P_{241}\Phi_x + P_{242}\frac{d\Phi_x}{dx} + P_{251}\Phi_\theta + P_{252}\frac{d\Phi_\theta}{dx} + +P_{253}\frac{d^2\Phi_\theta}{dx^2} = 0 \tag{24.b}$$

$$P_{311}U + P_{312}\frac{dU}{dx} + P_{321}V + P_{331}W + P_{332}\frac{dW}{dx} + P_{333}\frac{d^2W}{dx^2} + P_{341}\Phi_x + P_{342}\frac{d\Phi_x}{dx} + P_{351}\Phi_\theta = 0 \tag{24.c}$$

$$P_{411}U + P_{412}\frac{dU}{dx} + P_{413}\frac{d^2U}{dx^2} + P_{421}V + P_{422}\frac{dV}{dx} + P_{431}W + P_{432}\frac{dW}{dx} + P_{441}\Phi_x + P_{442}\frac{d\Phi_x}{dx} + P_{443}\frac{d^2\Phi_x}{dx^2} + P_{451}\Phi_\theta + P_{452}\frac{d\Phi_\theta}{dx} = 0 \quad (24.d)$$

$$P_{511}U + P_{512}\frac{dU}{dx} + P_{521}V + P_{522}\frac{dV}{dx} + P_{523}\frac{d^2V}{dx^2} + P_{531}W + P_{541}\Phi_x + P_{542}\frac{d\Phi_x}{dx} + P_{551}\Phi_\theta + P_{552}\frac{d\Phi_\theta}{dx} + +P_{553}\frac{d^2\Phi_\theta}{dx^2} = 0 \quad (24.e)$$

The coefficients P_{ijk} are provided in the Appendix. In this study some combinations of simply-supported (S) and clamped (C) boundary conditions have been used including CC, SS, CS and SC. The boundary conditions are expressed as:

$$\begin{aligned} C &: u_0^1 = v_0^1 = w_0^1 = \varphi_x^1 = \varphi_\theta^1 = 0 \\ S &: u_0^1 = v_0^1 = w_0^1 = M_{xx}^1 = \varphi_\theta^1 = 0 \end{aligned} \quad (25)$$

3.5. GDQ method

Generalized differential quadrature (GDQ) method has been widely utilized in research work due to high accuracy, convergence rate and flexibility in solving various problems [2,74,75]. Weight coefficients implemented in this method are only dependent on the grid points in the computational domain and the derivative order. Therefore, these nodal points can be chosen without limitation [76]. In this study, the GDQ method is used to solve the equations. Based on this method, the derivative of the m_{th} order of the function f(x) is obtained as a linear sum of the weight coefficients, and the nodal values of the function are expressed as:

$$\left.\frac{d^m f_{(x,t)}}{dx^m}\right|_{x=x_i} = \sum_{j=1}^{N} C_{ij}^m f_{(x_j,t)} \quad i = 1, 2, \ldots, N \quad (26)$$

In Eq. (26), N is the number of discretized nodal points in the x direction and C_{ij}^m are the weighting coefficients which can be calculated using Eq. (27).

$$C_{ij}^{(1)} = \begin{cases} \dfrac{M_{(x_i)}^{(i)}}{M_{(x_i)}^{(i)}(x_i - x_j)} & i \neq j \\ \dfrac{M^{(2)}(x_i)}{2M^{(i)}(x_i)} & i = j \end{cases} \quad (27)$$

where $M^{(i)}(x_i)$ can be obtained by Eq. (28).

$$M_{(x_k)}^{(1)} = \prod_{j=1, j\neq k}^{N} (x_k - x_j) \quad k = 1, 2, \ldots, N \quad (28)$$

The variable x with subscript i, j, and k represents the coordination of nodal points in the longitudinal direction of the cone The nodal points in Eq. (29) are defined based on the Chebyshev-Gauseg Lobato distribution, resulting in the enhanced convergence and stability of the solving procedure [77].

$$x_i = \frac{1 - \cos\left(\frac{i-1}{N-1}\pi\right)}{2} L \quad (29)$$

To apply the GDQ method to Eq. (24), the derivatives present in these equations must be discretized based on Eq. (26). By using this method, Eq. (24) are transformed into algebraic equations. To calculate the critical buckling load, the coefficients of these algebraic equations are placed in a matrix called the stiffness matrix. By computing the determinant of this matrix and setting it to zero, the critical buckling load is determined. In this study, MATLAB code is utilized to solve the bucking problem of the composite conical shells with the GDQ method.

4. Results and discussion

4.1. Experimental results

This section embraces the effects of sulfuric acid and nanoparticles including nano-silica and nano-clay on the mechanical, moisture and thermal properties of fabricated composites samples. To this end, glass/epoxy samples, reinforced by 3%wt. nanoparticles, were fabricated, and immersed into 5%wt. sulfuric acid solutions for durations of 1 and 3 months. Utilizing the tensile tests before and after immersion periods, the mechanical properties of nanocomposite samples required for the buckling analysis were obtained. Moreover, the coefficients of thermal and moisture expansion of nanocomposite samples were obtained through experimental procedures.

Table 1
Naming convention for fabricated glass/epoxy composite samples with nanoparticle reinforcements and sulfuric acid exposure.

Samples	Descriptions
P0	Glass/epoxy sample without nanoparticles, before sulfuric acid immersion
P1	Glass/epoxy sample without nanoparticles, after 1 month of sulfuric acid immersion
P3	Glass/epoxy sample without nanoparticles, after 3 months of sulfuric acid immersion
C0	Glass/epoxy sample reinforced with nano-clay, before sulfuric acid immersion
C1	Glass/epoxy sample reinforced with nano-clay, after 1 month of sulfuric acid immersion
C3	Glass/epoxy sample reinforced with nano-clay, after 3 months of sulfuric acid immersion
S0	Glass/epoxy sample reinforced with nano-silica, before sulfuric acid immersion
S1	Glass/epoxy sample reinforced with nano-silica, after 1 month of sulfuric acid immersion
S3	Glass/epoxy sample reinforced with nano-silica, after 3 months of sulfuric acid immersion

To distinguish various fabricated samples in the manuscript, a letter and a, number were used, in which the letter is either P, S, or C representing samples without nanoparticles, nano-silica, and nano-clay reinforced samples, respectively. The number in this naming convention is either 0, 1 or 3 which are denoted for sample before immersion, and samples after 1 or 3 months of immersion. The naming convection was clarified in Table 1.

4.1.1. Tensile test

In this section, the results of tensile tests were presented which have been used for calculating Poisson's ratio, Young's and shear modulus. As seen in Table 2 adding 3%wt. nano-clay particles improved Yong's modulus by 32.3 % and shear modulus by 22.2 %. Similarly, adding 3%wt. nano-silica increased these properties by 26.2 % and 5.4 % respectively. The main reason behind the mechanical properties improvement by adding 3%wt. nanoparticles is the immense interactions between epoxy resin and nanoparticles [78,79].

On the other hand, it was observed that the mechanical properties of nanocomposite samples drastically dropped by immersing into the sulfuric acid solution. Accordingly, in samples without nanoparticle reinforcement, the Young's modulus 5.9 % decreased after 1 month of immersion. This decrease reached 21.4 % after 3 months of immersion. Furthermore, the decreasing trends in Young's and shear modulus preserved for reinforced samples. Young's and shear modulus for nano-silica-reinforced samples after 3 months of immersion reduced by 25.1 % and 13.3 % respectively, while the reductions for nano-clay-reinforced particles were 6.8 % and 20.3 %.

Fig. 2 provides a comprehensive preview of the mechanical properties' reduction for various samples during distinct immersion periods. Corrosive environments can trigger degradation in both the matrix and reinforcement phases of composite materials. This degradation is caused by chemical interactions between the acidic solution and the composite, resulting in weakened fibers and a less robust composite material [80]. Based on Fig. 2, it can be understood that samples reinforced with nano-clay particles showed significantly better resistance against acidic environments compared to other samples. This may be attributed to the surface modifications in nanoparticles which leads to hydrophobicity [44].

4.1.2. Moisture absorption

As observed from Table 3, adding nano-clay particles to the epoxy matrix decreased the moisture content (ΔC) penetrated composite structure by 15.1 % for a 1-month immersion period and 46.9 % for a 3-month immersion period compared to the moisture absorption of pure samples. This can be explained by the hydrophobicity of organic clay nanoparticles, preventing the penetration of moisture into the composites' microstructure. In contrast, a negligible difference can be seen in the moisture absorption behavior of nano-silica-reinforced samples compared to the samples without reinforcement. This might be obtained due to the use of unmodified silica nanoparticles [81]. In this research, the amount of moisture absorption which was obtained by monitoring weight change in samples was not evaluated after three months. The reason behind this might be the domination of the corrosion phenomenon against the moisture penetration, which caused the samples to lose weight at higher rates after three months of immersion.

4.1.3. Coefficient of moisture expansion

Table 4 shows that introducing nano-clay and nano-silica particles reduced the coefficient of moisture expansion (CME) by 17.7 % and 23.3 % respectively. It may be concluded that adding nanoparticles, which improves mechanical properties, causes some reduction in longitudinal expansion of samples. Moreover, nanoparticle reinforcement prevented the moisture to penetrate the composite structure which may be another contributing reason. It is worth mentioning that due to using weave glass fabric, it was assumed in this study that the composite samples have quite the same coefficient of moisture expansion in both in-plane directions. The changes in the CME and moisture absorption with the addition of nanoparticles significantly influence the moisture-induced loading. According to Eq. (12), the moisture loading correlates directly with CME and the absorption rate. Therefore, by reducing moisture absorption and CME, the moisture-induced loading decreases, potentially increasing the thermal load required for buckling.

4.1.4. Glass transition temperature

The result of DSC test was illustrated in Table 5. It is obtained from this table that nanoparticles have negligible effects on glass transition temperature. However, in buckling analysis the temperature limit for all samples was set to 228 °C and this temperature was

Table 2
Mechanical properties of the samples during 0, 1, and 3 months of exposure to sulfuric acid.

Samples	$E_1 = E_2$ (GPa)	$G_{12} = G_{13} = G_{23}$ (GPa)	ν_{12}
P0	10.61	3.69	0.266
P1	9.98	3.72	0.266
P3	8.33	2.81	0.266
S0	13.4	3.89	0.266
S1	11.2	3.48	0.266
S3	10.03	3.37	0.266
C0	14.04	4.51	0.266
C1	13.6	4.09	0.266
C3	13.08	3.59	0.266

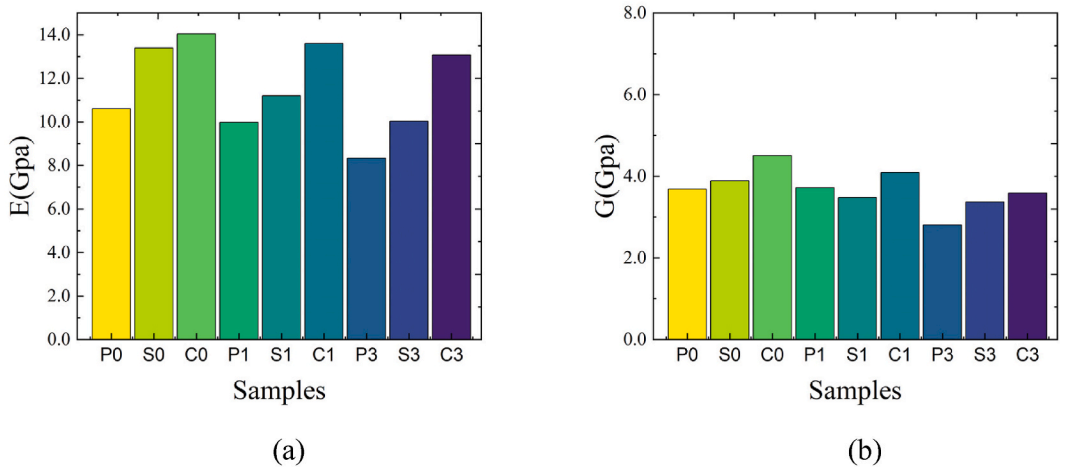

Fig. 2. Mechanical properties of the samples (a) Young's modulus (b) Shear modulus.

Table 3
The amount of moisture absorbed in sulfuric acid.

Samples	Immersion time	
	1 month	3 months
Glass/epoxy without nanoparticles	1.32	2.49
Glass/epoxy with 3%wt nano-clay	1.12	1.32
Glass/epoxy with 3%wt nano-silica	1.31	2.52

Table 4
Effect of nano-clay and nano-silica reinforcements on coefficient of moisture expansion (CME) in glass/epoxy composite samples.

Samples	$\beta_{11} = \beta_{22}$
Glass/epoxy without nanoparticles	0.090
Glass/epoxy with 3%wt nano-clay	0.074
Glass/epoxy with 3%wt nano-silica	0.069

Table 5
Glass transition temperature (Tg) of glass/epoxy composite samples with nano-clay and nano-silica reinforcements.

Samples	Glass transition temperature ($^{\circ}C$)
Glass/epoxy without nanoparticles	229.96
Glass/epoxy with 3%wt nano-clay	228.56
Glass/epoxy with 3%wt nano-silica	233.42

also selected as a maximum for dilatometer device.

4.1.5. Coefficient of thermal expansion

As described earlier, thermal bucking analysis of structures and calculation of critical buckling temperature necessitates to obtain the coefficient of thermal expansion (CTE) of composite samples. Calculation of this coefficient was done by averaging the slope of various sections of deflection-temperature plot. The averaging has been performed in two temperature intervals including 30 °C–50 °C and 30 °C–100 °C. The same procedure has been implemented by other researchers [42,76]. Table 6 presents the obtained coefficients of thermal expansion for fabricated samples. Additionally, Fig. 3 provides a comprehensive comparison of the thermal expansion coefficients.

The data provided in Fig. 3 shows a significant decrease in the CTE by introducing nanoparticle reinforcement. For example, in the samples S0 and C0, the coefficient of thermal expansion improved by 17.8 % and 28.3 % compared to the P0, respectively. As previously discussed, this change may be attributed to the difference between the thermal expansion coefficients of the nanoparticles and the composite matrix. It is worth noting that although adding nanoparticles has reduced the CTE, the optimal weight fraction of nanoparticles and the proper distribution of them in the matrix can be influential in preventing agglomerations. Similar results have been observed for various nanoparticles in the optimal weight percentage and proper dispersion [42,57,76,82].

On the other hand, it can be observed from the figure that immersing the samples in sulfuric acid solution resulted in increased coefficients of thermal expansion in such a way that after three months of immersion, the CTE of nano-clay and nano-silica reinforced samples increased by 72 % and 48.4 %, respectively. Moreover, it is seen that the CTEs of reinforced samples after each exposure period have slightly the same value. This may present the drastic influence of sulfuric acid that faded the improving effects of adding nanoparticles.

4.2. Verification and convergence study

The present study benefits from the GDQ numerical method to solve the governing equations of conical and cylindrical shells and calculate the critical buckling temperature. In this section, first, the convergence of the numerical procedure is presented which demonstrates the efficiency of the GDQ for thermal buckling analysis and then, the verification study was provided through several examples to compare and validate the results of implemented Matlab code with previous studies.

4.2.1. Convergence

Table 7 demonstrates the critical buckling temperatures of conical shell with properties of P3 samples for various types of boundary conditions including S-S, C-C, C-S and S-C. As seen in this table, the critical buckling temperature converges as the number of grid points reaches 15 in the x direction.

4.2.2. Verification

Regarding the verification study, in the first example the critical buckling temperature of conical shells with CC and SS boundary conditions and various semi-vertex cone angles was compared with the studies of Sing and Babu [83], Patel [84], and Mirzaei [66]. Both Patel and Mirzaei's studies utilized the First-order Shear Deformation Theory (FSDT), while Sing and Babu's anslysis was based on the Higher-order Shear Deformation Theory (HSDT). The results were provided in Table 8 for two different lamination sequences including [0/90] and $[0/90]_4$. Upon comparing the data presented in this table with the results of Mirzaei [66], it is observed that the deviation between the results for different cone angles is less than 1 %. This indicates a high level of agreement in the obtained results, highlighting the accuracy of the implemented procedure.

Table 6
Effect of nano-clay and nano-silica reinforcements on coefficient of thermal expansion (CTE) in glass/epoxy composite samples $\left(\frac{10^{-6}}{^{\circ}C}\right)$.

Samples	Value
P0	9.04
P1	10.64
P3	12.83
S0	7.43
S1	9.84
S3	11.03
C0	6.48
C1	9.47
C3	11.15

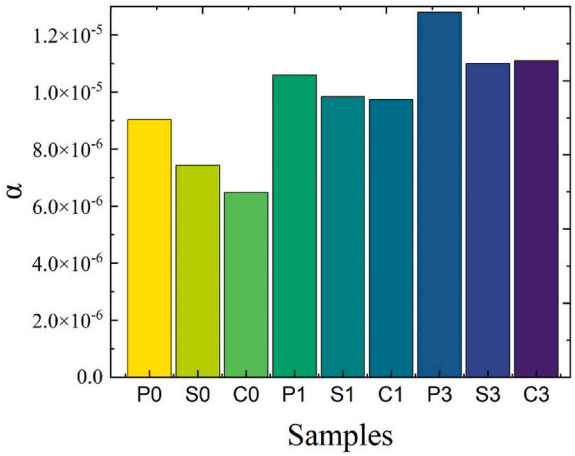

Fig. 3. Coefficient of thermal expansion of the samples during 0, 1, and 3 months of exposure to sulfuric acid.

Table 7
Convergence of critical buckling temperature of the conical shell for P3 with GDQ numerical method under different boundary conditions. ($\delta = 30^{\circ}$, $L/R_0 = 1$, $R_0/h = 1/500$).

N	S-S	C-C	C-S	S-C
7	66.05 (19)	70.32 (19)	68.27 (20)	67.28 (19)
9	61.10 (20)	62.78 (20)	61.16 (22)	61.70 (20)
11	59.66 (21)	60.32 (21)	59.77 (22)	59.80 (21)
13	59.39 (21)	59.55 (21)	59.47 (22)	59.40 (21)
15	59.21 (21)	59.34 (21)	59.24 (22)	59.21 (21)
17	59.21 (21)	59.34 (21)	59.24 (22)	59.21 (21)
19	59.21 (21)	59.34 (21)	59.24 (22)	59.21 (21)

Table 8
Comparison of critical buckling temperature parameter $\lambda cr = \Delta T_{cr}\alpha_{11}R_1/h$ for C-C conical shells with various semi-vertex angles ($R_1/h = 100$ and $L/R_0 = 1$), $\left(E_{11} = 172.5\ \text{GPa}, E_{22} = 6.89\ \text{GPa}, G_{12} = G_{13} = 3.445\ \text{GPa}, G_{23} = 1.378\ \text{GPa}, \nu_{12} = 0.25, \alpha_{11} = 6.3{*}10^{-6}\frac{1}{\text{K}}, \alpha_{22} = 18.9{*}10^{-6}\frac{1}{\text{K}}\right)$.

$\delta(^{\circ})$	[0/90]				$[0/90]_4$			
	Sing [83]	Patel [84]	Mirzaei [66]	Present	Sing [83]	Patel [84]	Mirzaei [66]	Present
0	0.1049	0.1014	0.1017	0.1013	0.1640	0.1638	0.1638	0.1636
15	0.0823	0.0890	0.0887	0.0882	0.1463	0.1453	0.1453	0.1451
30	0.0770	0.0750	0.0739	0.0737	0.1265	0.1255	0.1258	0.1255
45	0.0635	0.0595	0.0594	0.0598	0.1036	0.1041	0.0989	0.0989
60	0.0468	0.0447	0.0432	0.0435	0.0807	0.0824	0.0819	0.0811

The second example compares the results of critical buckling temperature parameter ($\lambda cr = \Delta T_{cr}\alpha_{11}R_1/h$) in various radius to thickness ratio (R_0/h) and length to radius ration (L/R_0) of the shell with those of obtained by Patel [84] in *SS* boundary condition. According to the data in Table 9 the deviation of results is less than 5 % which is a satisfying achievement.

The third example investigates the critical buckling temperature of the conical composite shells with temperature-dependent properties and CC boundary condition. The results provided in Table 10 were compared with those of Kiani [70], Akbari [71] and Bhangale [85] and a good agreement was achieved. Temperature-dependent material properties were employed based on Eq. (29). Both Bhangale and Kiani employed the FSDT in their studies, whereas Akbari's research utilized the Classical Deformation Theory (CST).

$$\begin{aligned} E(T) &= 201.04\left(1 + 3.079{*}T{*}10^{-4} - 6.534{*}T^2{*}10^{-7}\right)\ GPa \\ \alpha(T) &= 12.330\left(1 + 8.086{*}T{*}10^{-4}\right){*}10^{-6} \\ \nu &= 0.3262\left(1 - 2.002{*}T{*}10^{-4} + 3.797{*}T^2{*}10^{-7}\right) \end{aligned} \tag{30}$$

Table 9
Comparison of critical buckling temperature parameter $\lambda cr = \Delta T_{cr}\alpha_{11}R_1/h$ for S-S conical shells with various semi-vertex angles and L/R_0, R_0/h ($E_{11} = 172.5\ \text{GPa}, E_{22} = 6.89\ \text{GPa}, G_{12} = G_{13} = 3.445\ \text{GPa}, G_{23} = 1.378\ \text{GPa}, \nu_{12} = 0.25, \alpha_{11} = 6.3{*}10^{-6}\frac{1}{\text{K}}, \alpha_{22} = 18.9{*}10^{-6}\frac{1}{\text{K}}$).

R_0/h	L/R_0	$\delta(^\circ)$	[0,90]		$[0,90]_4$		$[0,90]_{2s}$	
			Patel [84]	Present	Patel [84]	Present	Patel [84]	Present
10	5	0	0.0847	0.0827	0.1297	0.1317	0.1340	0.1341
		15	0.0544	0.0544	0.0807	0.0819	0.0838	0.0839
		30	0.0395	0.0398	0.0594	0.0608	0.0606	0.0602
		45	0.0286	0.0291	0.0437	0.0446	0.0457	0.0455
		60	0.0190	0.0196	0.0301	0.0302	0.0327	0.0311
100	1	0	0.0977	0.0977	0.1433	0.1443	0.1442	0.1424
		15	0.0832	0.0838	0.1217	0.1229	0.1271	0.1260
		30	0.0672	0.0687	0.1005	0.1022	0.1080	0.1065
		45	0.0506	0.0523	0.0786	0.0808	0.0871	0.0819
		60	0.0350	0.0365	0.0580	0.0604	0.0656	0.0630
	0.5	0	0.1008	0.1065	0.1484	0.1499	0.1489	0.1443
		15	0.0936	0.0995	0.1332	0.1352	0.1362	0.1329
		30	0.0839	0.0896	0.1130	0.1157	0.1177	0.1153
		45	0.0727	0.0735	0.0900	0.0937	0.0958	0.0951
		60	0.0613	0.0574	0.0673	0.0686	0.0736	0.0743

Table 10
Comparison of critical buckling temperature of SUS304 conical shell with temperature-dependent material properties.

	Kiani [70]	Akbari [71]	Bhangale [85]	Present
$\delta = 15^\circ$ $R_0/h = 252.5573$	423.17	423.23	424.11	423.23
$\delta = 30^\circ$ $R_0/h = 215.8026$	412.99	413.60	413.74	413.57

4.3. Numerical results

Table 11 presents the influence of nano-silica and nano-clay in the matrix of epoxy/glass nanocomposites on the critical buckling temperature of composite conical shells. In this regard, the geometrical parameters of the shell were considered as $R_0/h = 1/500$, $L/R_0 = 1$, and $\delta = 30^\circ$. In general, it is obtained that adding nanoparticles can improve the critical buckling temperature of the structure, which results in more stability. As presented in the table, adding nano-silica particles caused 11.5 % improvement in critical buckling temperature of the shell, while nano-clay particles were responsible for 34.2 % increase in the same parameter. The reason behind the significant impact of nano-clay particles may be explained by the considerably better mechanical and thermal properties in samples reinforced by nano-clay. These changes demonstrate that adding nanoparticles into the composite matrix can elevate the critical

Table 11
The effect of adding nano-silica, and nano-clay on the critical buckling temperature of the composite conical shell with different boundary conditions ($\delta = 30^\circ$, $L/R_0 = 1$, $R_0/h = 1/500$).

B.C	P0	S0	C0	Improvement (%)	
				Nano-silica	Nano-clay
CC	87.77 (22)	97.88 (21)	117.87 (21)	11.51	34.29
SS	87.60 (22)	97.55 (21)	117.56 (21)	11.35	34.20
CS	87.64 (22)	97.69 (21)	117.67 (21)	11.46	34.26
SC	87.62 (22)	97.60 (21)	117.62 (21)	11.39	34.23

Table 12
The effect of adding nano-silica, and nano-clay on the critical buckling temperature of the composite conical shell immersed in sulfuric acid for 3 months with different boundary conditions. ($\delta = 30^\circ$, $L/R_0 = 1$, $R_0/h = 1/500$).

B.C	P3	S3	C3	Improvement (%)	
				Nano-silica	Nano-clay
CC	59.20 (22)	69.32 (21)	62.64 (21)	17.05	5.81
SS	59.07 (22)	69.17 (21)	62.41 (21)	17.09	5.65
CS	59.11 (22)	69.21 (21)	62.51 (21)	17.08	5.75
SC	59.08 (22)	69.19 (21)	62.46 (21)	17.11	5.72

buckling temperature. Thereby enhancing the stability of the conical shell. Moreover, it was observed that changes in mechanical and thermal properties due to adding nanoparticles led to some change in the circumferential wave number (n) from 22 to 21.

The effects of three-month exposure of composite conical shells to acidic environment were presented in Table 12. The same geometrical parameters including $R_0/h = 1/500$, $L/R_0 = 1$, and $\delta = 30^\circ$ were implemented for buckling analysis in this section. It is obtained from Table 12 that composite shells with nanoparticle reinforcement possess higher critical buckling temperature compared to the pure samples, which shows the significant impact of employing nanoparticles in corrosive environments. Comparing the data provided in Tables 11 and 12, it can be seen that the effectiveness of introducing nanoparticles has been changed in the presence of acidic environment. The reason behind this may be the relative analogy in the CTE for the reinforced and unreinforced samples after exposure to acidic condition. Herein, it is observed that the improvement percentage of critical buckling temperature in the presence of nano-silica (S3) is more than nano-clay (C3) as opposed to the samples before exposure to acidic condition (S0 and C0). This observation can be explained by the CTE related to the S3 samples that is more than that of C3 samples. It is worth noting that the impact of various boundary conditions was negligible, so their comparison was disregarded in this manuscript.

Fig. 4 illustrates the effect of changes in the semi-vertex angle of the cone and immersion period on the critical buckling temperature of nanocomposite conical shells for various types of nanoparticle reinforcement. In general, a downward trend can be seen by increasing the semi-vertex angle of the conical shell which belongs to the change in the stiffness of the structure. Furthermore, there can be seen a downward shift in the curves associated with the exposure period of composite shells to acidic condition. It can be explained that exposure of composite shells to acidic condition may result in decreased mechanical properties, increased coefficient of thermal expansion and forming in-plane hygric loads. Moreover, it is seen that the drop in critical buckling temperature was significantly higher in reinforced samples compared to the pure samples.

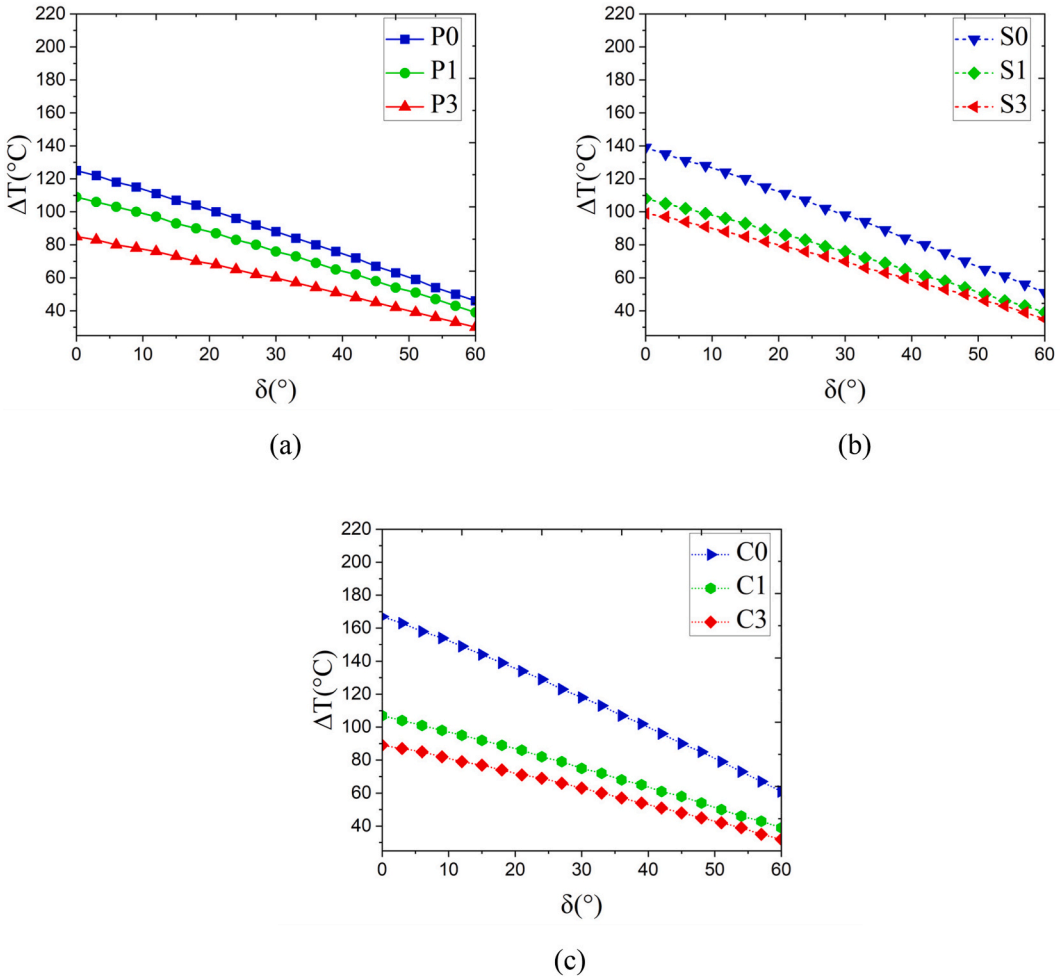

Fig. 4. Effect of the semi-vertex cone ang and immersion time the critical buckling temperature of nanocomposite conical shells ($R_0/h = 1/500$, $L/R_0 = 1$).

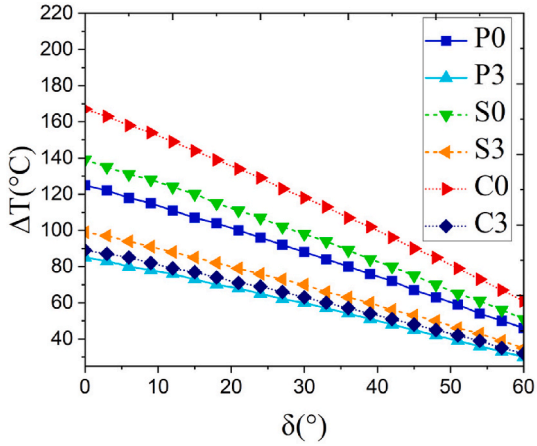

Fig. 5. Variation of critical buckling temperature terms of cone angle for various samples before and after 3-month of exposure to acidic environment ($R_0/h = 1/500$, $L/R_0 = 1$).

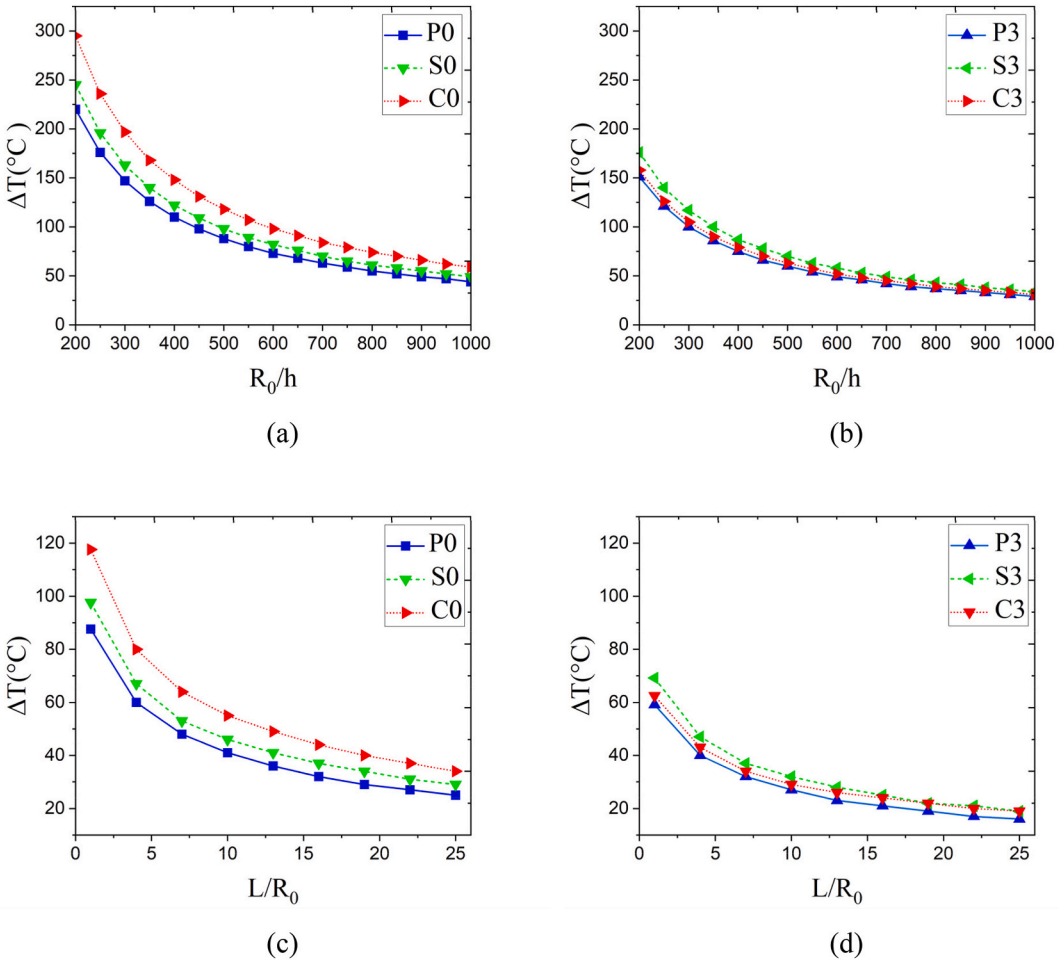

Fig. 6. The effect of R_0/h and L/R_0 on the critical buckling temperature of the nanoparticle-reinforced composite shell ($\delta = 30°$, Boundary conditions: S-S, (a) and (b) $L/R_0 = 1$, (c) and (d) $R_0/h = 1/500$.

Fig. 5 provides a general comparison of ΔT_{cr} in terms of cone angle between various types of nanoparticle reinforcement before and after 3-month of exposure to acidic environment. It is observed that before exposure (S0 and C0), the composite shell has strongly higher critical buckling temperature (ΔT_{cr}) compared to P0. However, after exposure to acidic environment, the ΔT_{cr} for C3, S3 and P3 samples are quite similar, which is due to the analogous coefficient of thermal expansion. In fact, the destructive effect of sulfuric acid on ΔT_{cr} is dominantly effective compared to the positive impact of nanoparticles.

Fig. 6 has been provided to highlight the effects of geometric parameters on the critical buckling temperature of the composite conical shells. As seen, by increasing the L/R_0 and R_0/h ratios, the critical buckling temperature of the shells decreases, which leads to more instability in the structure. Moreover, it was found that adding nanoparticles regardless of geometric parameters increases the critical buckling temperature. Furthermore, the influence of an acidic environment can be observed in Fig. 6, where the distances between the graphs in Fig. 6a and 6c are significantly greater than those of Fig. 6b and 6d. This observation indicates that exposure to acidic environments can diminish the effect of nanoparticles in enhancing the critical buckling temperature.

5. Conclusion

This research studied the detrimental effects of acid penetration and temperature increase on the buckling behavior of conical composite shells. The study investigated the impact of incorporating 3%wt. nano-silica or nano-clay particles on the mechanical, moisture and thermal properties, and the buckling behavior of the structure using experimentally obtained material properties. To achieve this, nanoparticle-reinforced composite samples were fabricated, and their mechanical and hygrothermal properties were determined through experimental tests while samples exposed to sulfuric acid solution. The governing equations for conical shells under hygrothermal loading were derived using the FSDT theory and the buckling loads were obtained from pre-buckling analysis. By incorporating the experimentally obtained material properties into the governing equations, the hygrothermal buckling problem of the reinforced composite shell was solved using the GDQ method.

Results of the study are presented as follows:

It was found that nanoparticles can be effective in the moisture properties of the samples including moisture absorption and the coefficient of moisture expansion. It was shown that introducing nano-clay and nano-silica particles reduced the coefficient of moisture expansion by 17.8 % and 23.3 % respectively. A significant decrease in the coefficient of thermal expansion was observed by adding nanoparticles. For example, the CTE of samples containing nano-silica and nano-clay before immersion was reduced by 17.8 % and 28.3 %, respectively. In contrast, immersing the samples in sulfuric acid solution resulted in increased CTE. For instance, after three months of immersion, the CTE of nano-clay and nano-silica reinforced samples increased by 72 % and 48.4 %, respectively. It was observed that nanoparticles could improve the stability of the structure by increasing the critical buckling temperature. Herein, the nano-clay reinforced samples had the highest critical buckling temperature. As an example, adding nano-silica particles caused 11.5 % improvement in critical buckling temperature of the shell, while nano-clay particles were responsible for 34.2 % increase. Additionally, it was seen that the effectiveness of nanoparticles has faded in the presence of acidic environment due to the negligible difference in the CTE of the reinforced and unreinforced samples after exposure to acidic condition.

The acidic environment may affect the structure's buckling behavior in two ways. First, the corrosion which affects the mechanical and thermal properties of composite materials. Second, the acid penetration through the composite media may cause hygric loads. Introducing nanoparticles can be significantly influential on the negative impact of acid exposure in both improving the mechanical properties and preventing acid penetration, as well as changing the coefficient of moisture and thermal expansion. Changing the semi-vertex angle of the cone reduced the critical buckling temperature, which is associated with the change in the stiffness of the structure. Furthermore, changing other geometrical parameters including L/R_0 and R_0/h ratios can affect the critical buckling temperature of the shell as some decrease was observed by increasing those parameters. It can be observed that an effective way of promoting the buckling behavior of the shell is controlling the geometrical parameters.

Data availability statement

The datasets generated and/or analyzed during the current study are available from the corresponding author on reasonable request.

CRediT authorship contribution statement

Seyed Masoud Montazeri: Writing – original draft, Methodology. **Saeed Saber-Samandari:** Writing – review & editing, Supervision, Formal analysis, Conceptualization. **Seyed Ali Sadough Vanini:** Supervision.

Declaration of competing interest

The authors declare that they have no known competing financial interests or personal relationships that could have appeared to influence the work reported in this paper.

Appendix

Eq (A.1) to A.5 present the governing equations of the composite conical shells in terms of displacement components, and they are derived based on FSDT, and by utilizing a pre-buckling analysis.

$$A_{11}\frac{\partial^2 u}{\partial x^2}+\left(\frac{A_{11}\sin(\delta)}{r(x)}\right)\frac{\partial u}{\partial x}+\frac{A_{66}}{r^2(x)}\frac{\partial^2 u}{\partial \theta^2}-\frac{A_{22}\sin^2(\delta)}{r^2(x)}u+\frac{(A_{66}+A_{12})}{r(x)}\frac{\partial^2 v}{\partial x\partial\theta}-\frac{(A_{66}+A_{22})\sin(\delta)}{r^2(x)}\frac{\partial v}{\partial\theta}+\frac{A_{12}\cos(\delta)}{r(x)}\frac{\partial w}{\partial x}$$
$$-\frac{A_{22}\cos(\delta)\sin(\delta)}{r^2(x)}w+B_{11}\frac{\partial^2\varphi_x}{\partial x^2}+\frac{B_{11}\sin(\delta)}{r(x)}\frac{\partial\varphi_x}{\partial x}-\frac{B_{22}\sin^2(\delta)}{r^2(x)}\varphi_x+\frac{B_{66}}{r^2(x)}\frac{\partial^2\varphi_x}{\partial\theta^2}+\frac{(B_{66}+B_{12})}{r(x)}\frac{\partial^2\varphi_\theta}{\partial x\partial\theta}-\frac{(B_{66}+B_{22})\sin(\delta)}{r^2(x)}\frac{\partial\varphi_\theta}{\partial\theta}=0 \tag{A-1}$$

$$\frac{(A_{66}+A_{12})}{r(x)}\frac{\partial^2 u}{\partial x\partial\theta}+\frac{(A_{66}+A_{22})\sin(\delta)}{r^2(x)}\frac{\partial u}{\partial\theta}+A_{66}\frac{\partial^2 v}{\partial x^2}+\frac{A_{66}\sin(\delta)}{r(x)}\frac{\partial v}{\partial x}+\frac{A_{22}}{r^2(x)}\frac{\partial^2 v}{\partial\theta^2}-\left(\frac{A_{66}\sin^2(\delta)}{r^2(x)}-\frac{K_sA_{44}\cos^2(\delta)}{r^2(x)}\right)v$$
$$+\left(\frac{A_{22}\cos(\delta)}{r^2(x)}+\frac{K_sA_{44}\cos(\delta)}{r^2(x)}\right)\frac{\partial w}{\partial\theta}+\frac{(B_{66}+B_{12})}{r(x)}\frac{\partial^2\varphi_x}{\partial x\partial\theta}+\frac{(B_{66}+B_{22})\sin(\delta)}{r^2(x)}\frac{\partial\varphi_x}{\partial\theta} \tag{A-2}$$
$$+B_{66}\frac{\partial^2\varphi_\theta}{\partial x^2}+\frac{B_{66}\sin(\delta)}{r(x)}\frac{\partial\varphi_\theta}{\partial x}+\frac{B_{22}}{r^2(x)}\frac{\partial^2\varphi_\theta}{\partial\theta^2}+\left(\frac{K_sA_{44}\cos(\delta)}{r(x)}-\frac{B_{66}\sin^2(\delta)}{r^2(x)}\right)\varphi_\theta=0$$

$$-\frac{A_{12}\cos(\delta)}{r(x)}\frac{\partial u}{\partial x}-\frac{A_{22}\cos(\delta)\sin(\delta)}{r^2(x)}u+\left(\frac{K_sA_{44}+A_{22}}{r^2(x)}(\cos(\delta))\right)\frac{\partial v}{\partial\theta}+K_sA_{55}\frac{\partial^2 w}{\partial x^2}+\frac{K_sA_{55}\sin(\delta)}{r(x)}\frac{\partial w}{\partial x}+\frac{K_sA_{44}}{r^2(x)}\frac{\partial^2 w}{\partial\theta^2}$$
$$-\frac{A_{22}\cos^2(\delta)}{r^2(x)}w+\frac{L\sin(\delta)\left(A_{22}N^{TC}_{xx}-A_{12}N^{TC}_{\theta\theta}\right)}{r(x)A_{22}Ln\left(1+\frac{L\sin(\delta)}{R_0}\right)}w^1_{0,xx}+\left(K_sA_{55}-\frac{B_{12}\cos(\delta)}{r(x)}\right)\frac{\partial\varphi_x}{\partial x}+\left(\frac{K_sA_{55}\sin(\delta)}{r(x)}\right.$$
$$\left.-\frac{B_{22}\sin(\delta)\cos(\delta)}{r^2(x)}\right)\varphi_x+\left(\frac{K_sA_{44}r(x)-B_{22}\cos(\delta)}{r^2(x)}\right)\frac{\partial\varphi_\theta}{\partial\theta}=0 \tag{A-3}$$

$$B_{11}\frac{\partial^2 u}{\partial x^2}+\left(\frac{B_{11}\sin(\delta)}{r(x)}\right)\frac{\partial u}{\partial x}+\frac{B_{66}}{r^2(x)}\frac{\partial^2 u}{\partial\theta^2}-\frac{B_{22}\sin^2(\delta)}{r^2(x)}u+\frac{(B_{66}+B_{12})}{r(x)}\frac{\partial^2 v}{\partial x\partial\theta}-\left(\frac{(B_{22}+B_{66})\sin(\delta)}{r^2(x)}\right)\frac{\partial v}{\partial\theta}+\left(\frac{B_{12}\cos(\delta)}{r(x)}-K_sA_{55}\right)\frac{\partial w}{\partial x}$$
$$-\frac{B_{22}\cos(\delta)\sin(\delta)}{r^2(x)}w+D_{11}\frac{\partial^2\varphi_x}{\partial x^2}+\frac{D_{11}\sin(\delta)}{r(x)}\frac{\partial\varphi_x}{\partial x}-\left(\frac{D_{22}\sin^2(\delta)}{r^2(x)}+K_sA_{55}\right)\varphi_x+\frac{D_{66}}{r^2(x)}\frac{\partial^2\varphi_x}{\partial\theta^2}+\frac{(D_{66}+D_{12})}{r(x)}\frac{\partial^2\varphi_\theta}{\partial x\partial\theta}$$
$$-\frac{(D_{66}+D_{22})\sin(\delta)}{r^2(x)}\frac{\partial\varphi_\theta}{\partial\theta}=0 \tag{A-4}$$

$$\frac{(B_{66}+B_{12})}{r(x)}\frac{\partial^2 u}{\partial x\partial\theta}+\frac{(B_{66}+B_{22})\sin(\delta)}{r^2(x)}\frac{\partial u}{\partial\theta}+B_{66}\frac{\partial^2 v}{\partial x^2}+\frac{B_{66}\sin(\delta)}{r(x)}\frac{\partial v}{\partial x}+\frac{B_{22}}{r^2(x)}\frac{\partial^2 v}{\partial\theta^2}-\left(\frac{B_{66}\sin^2(\delta)}{r^2(x)}-\frac{K_sA_{44}\cos(\delta)}{r(x)}\right)v+\left(\frac{B_{22}\cos(\delta)}{r^2(x)}\right.$$
$$\left.-\frac{K_sA_{44}}{r(x)}\right)\frac{\partial w}{\partial\theta}+\frac{(D_{66}+D_{12})}{r(x)}\frac{\partial^2\varphi_x}{\partial x\partial\theta}+\frac{(D_{22}+D_{66})\sin(\delta)}{r^2(x)}\frac{\partial\varphi_x}{\partial\theta}+D_{66}\frac{\partial^2\varphi_\theta}{\partial x^2}+\frac{D_{66}\sin(\delta)}{r(x)}\frac{\partial\varphi_\theta}{\partial x}+\frac{D_{22}}{r^2(x)}\frac{\partial^2\varphi_\theta}{\partial\theta^2}$$
$$-\left(K_sA_{44}+\frac{D_{66}\sin^2(\delta)}{r^2(x)}\right)\varphi_\theta=0 \tag{A-5}$$

The expressions below are the constant coefficients utilized within Eq. (24) in the manuscript.

$$P_{111} = -\frac{A_{66}n^2}{r^2(x)} - \frac{A_{22}\,sin^2(\delta)}{r^2(x)}, P_{112} = \frac{A_{11}\,sin(\delta)}{r(x)}, P_{113} = A_{11}$$

$$, P_{121} = -\frac{(A_{66} + A_{22})n\,sin(\delta)}{r^2(x)}, P_{122} = \frac{(A_{66} + A_{12})n\,sin(\delta)}{r(x)}$$

$$, P_{131} = -\frac{A_{22}\,cos(\delta)sin(\delta)}{r^2(x)}, P_{132} = \frac{A_{12}\,cos(\delta)}{r(x)}$$

$$, P_{141} = -\frac{B_{22}\,sin^2(\delta)}{r^2(x)} - \frac{B_{66}}{r^2(x)}n^2, P_{142} = \frac{B_{11}\,sin(\delta)}{r(x)}, P_{143} = B_{11}$$

$$, P_{151} = -\frac{(B_{66} + B_{22})sin(\delta)}{r^2(x)}n, P_{152} = \frac{(B_{66} + B_{12})}{r(x)}n$$

$$, P_{211} = -\frac{(A_{66} + A_{22})sin(\delta)}{r^2(x)}n, P_{212} = -\frac{(A_{66} + A_{12})}{r(x)}n$$

$$, P_{221} = -\frac{A_{22}}{r^2(x)}n^2 - \left(\frac{A_{66}\,sin^2(\delta)}{r^2(x)} - \frac{K_sA_{44}\,cos^2(\delta)}{r^2(x)}\right)$$

$$, P_{222} = \frac{A_{66}\,sin(\delta)}{r(x)}, P_{223} = A_{66}$$

$$, P_{231} = -\left(\frac{A_{22}\,cos(\delta)}{r^2(x)} + \frac{K_sA_{44}\,cos(\delta)}{r^2(x)}\right)n, P_{241} = -\frac{(B_{66} + B_{22})sin(\delta)}{r^2(x)}$$

$$, P_{242} = -\frac{(B_{66} + B_{12})}{r(x)}n$$

$$, P_{251} = \left(\frac{K_sA_{44}\,cos(\delta)}{r(x)} - \frac{B_{66}\,sin^2(\delta)}{r^2(x)}\right) - \frac{B_{22}}{r^2(x)}n^2, P_{252} = \frac{B_{66}\,sin(\delta)}{r(x)}$$

$$, P_{253} = B_{66}, P_{311} = -\frac{A_{22}\,cos(\delta)\,sin(\delta)}{r^2(x)}, P_{312} = -\frac{A_{12}\,cos(\delta)}{r(x)}$$

$$, P_{321} = \left(\frac{K_sA_{44} + A_{22}}{r^2(x)}cos(\delta)\right)n$$

$$, P_{331} = -\frac{A_{22}cos^2(\delta)}{r^2(x)} - \frac{K_sA_{44}}{r^2(x)}n^2$$

$$, P_{332} = \frac{K_sA_{55}\,sin(\delta)}{r(x)}$$

$$, P_{333} = \frac{L\,sin(\delta)\left(A_{22}N_{xx}^{TC} - A_{12}\,N_{\theta\theta}^{TC}\right)}{r(x)\,A_{22}\,Ln\left(1 + \frac{L\,sin(\delta)}{R_0}\right)} + K_sA_{55}$$

$$, P_{341} = \left(\frac{K_sA_{55}\,sin(\delta)}{r(x)} - \frac{B_{22}\,sin(\delta)cos(\delta)}{r^2(x)}\right)$$

$$, P_{342} = \left(K_sA_{55} - \frac{B_{12}\,cos(\delta)}{r(x)}\right), P_{351} = \left(\frac{K_sA_{44}r(x) - B_{22}\,cos(\delta)}{r^2(x)}\right)n$$

$$P_{411} = -\frac{B_{66}}{r^2(x)}n^2 - \frac{B_{22}\,sin^2(\delta)}{r^2(x)}, P_{412} = \frac{B_{11}\,sin(\delta)}{r(x)}, P_{413} = B_{11}$$

$$, P_{421} = -\frac{(B_{22} + B_{66})\,sin(\delta)}{r^2(x)}n, P_{422} = \frac{(B_{66} + B_{12})sin(\delta)}{r(x)}n$$

$$, P_{431} = -\frac{B_{22}\,cos(\delta)sin(\delta)}{r(x)}, P_{432} = \frac{B_{12}\,cos(\delta)}{r(x)} - K_sA_{55}$$

$$, P_{441} = -\left(\frac{D_{22}\,sin^2(\delta)}{r^2(x)} + K_sA_{55}\right) - \frac{D_{66}}{r^2(x)}n^2, P_{442} = \frac{D_{11}\,sin(\delta)}{r(x)}$$

$$, P_{443} = D_{11}, P_{451} = \frac{(D_{66} + D_{22})sin(\delta)}{r^2(x)}n^2, P_{452} = \frac{(D_{66} + D_{12})}{r(x)}n$$

$$P_{511} = -\frac{(B_{66} + B_{22})sin(\delta)}{r^2(x)}n, P_{512} = -\frac{(B_{66} + B_{12})}{r(x)}n,$$

$$P_{521} = -\frac{B_{22}}{r^2(x)}n^2 - \left(\frac{B_{66}\,sin^2(\delta)}{r^2(x)} - \frac{K_sA_{44}r(x)cos(\delta)}{r^2(x)}\right)$$

$$, P_{522} = \frac{B_{66}\,sin(\delta)}{r(x)}, P_{523} = B_{66}, P_{531} = \left(\frac{B_{22}\,cos(\delta)}{r^2(x)} - \frac{K_sA_{44}}{r(x)}\right)n,$$

$$P_{541} = -\frac{(D_{22} + D_{66})sin(\delta)}{r^2(x)}n^2, P_{542} = -\frac{(D_{66} + D_{12})}{r(x)}\,n$$

$$, P_{551} = -\left(K_sA_{44} + \frac{D_{66}\,sin^2(\delta)}{r^2(x)} - \frac{D_{22}}{r^2(x)}n^2\right), P_{552} = \frac{D_{66}\,sin(\delta)}{r(x)}$$

$$, P_{553} = D_{66}$$

References

[1] P. Feng, et al., Effects of corrosive environments on properties of pultruded GFRP plates, Compos. B Eng. 67 (2014) 427–433.
[2] S. Kamarian, M. Bodaghi, J.i. Song, Hygrothermal effects on the buckling of soft-core sandwich plates with composite layered face sheets, Polym. Compos. 41 (10) (2020) 4144–4169.
[3] M. Alinia, S. Saber-Samandari, S.A. Sadough Vanini, On the mechanical properties and vibrational characteristics of the nanoparticle-reinforced composite cylindrical panels in the acidic environment: Numerical and experimental investigation, Journal of Reinforced Plastics and Composites (2023) 07316844231197256.
[4] F. Rahmani, et al., Experimental and analytical investigation on forced and free vibration of sandwich structures with reinforced composite faces in an acidic environment, Heliyon 9 (10) (2023) e20864.
[5] N. Mortas, et al., Effect of corrosive solutions on composites laminates subjected to low velocity impact loading, Compos. Struct. 108 (2014) 205–211.
[6] J.J. Schubbe, S.H. Bolstad, S. Reyes, Fatigue crack growth behavior of aerospace and ship-grade aluminum repaired with composite patches in a corrosive environment, Compos. Struct. 144 (2016) 44–56.
[7] A. Amaro, et al., Effect of different acid solutions on glass/epoxy composites, J. Reinforc. Plast. Compos. 32 (14) (2013) 1018–1029.
[8] S. Ebadzadsahraei, M. Hassan Vakili, Comparison of corrosion resistance of fiberglass/epoxy and fiberglass/polyester composite pipes for application in natural gas transportation, J. Pipeline Syst. Eng. Pract. 10 (3) (2019) 6019001.
[9] F. Rahmani, et al., Effect of corrosive environment on mechanical properties of polymer-based nanocomposite: analytical and experimental study, Mater. Today Commun. 36 (2023) 106544.
[10] N. Jiang, et al., Hygrothermal aging and structural damage of a jute/poly (lactic acid)(PLA) composite observed by X-ray tomography, Compos. Sci. Technol. 173 (2019) 15–23.
[11] H. Dehghanian, S.M.H. Farrash, M. Jafari, Effect of moisture absorption on the flexural strength of phenolic matrix composites reinforced with glass fibers and aluminum oxide nanoparticles, Polym. Compos. 45 (1) (2023) 1–8.
[12] A.P. Chakraverty, et al., Sea water ageing of GFRP composites and the dissolved salts, in: IOP Conference Series: Materials Science and Engineering, IOP Publishing, 2015.
[13] R. Ansari, J. Torabi, E. Hasrati, Postbuckling analysis of axially-loaded functionally graded GPL-reinforced composite conical shells, Thin-Walled Struct. 148 (2020) 106594.
[14] Y. Feng, et al., Investigation on the buckling and postbuckling performance of aero stiffened composite panels under axial compression, Polym. Compos. 39 (7) (2018) 2547–2559.
[15] X. Zhou, et al., Buckling analysis on resin base laminated plate reinforced with uniform and functional gradient distribution of carbon fiber in thermal environment, Polymers 15 (9) (2023) 2086.
[16] R.B. Mahani, et al., Thermal buckling of laminated Nano-Composite conical shell reinforced with graphene platelets, Thin-Walled Struct. 155 (2020) 106913.
[17] M. Avey, N. Fantuzzi, A. Sofiyev, On the solution of thermal buckling problem of moderately thick laminated conical shells containing carbon nanotube originating layers, Materials 15 (21) (2022) 7427.
[18] O. Barton Jr., Eigensensitivity analysis of moisture-related buckling of marine composite panels, Ocean Eng. 34 (11–12) (2007) 1543–1551.
[19] M. Babaei, F. Kiarasi, K. Asemi, Torsional buckling response of FG porous thick truncated conical shell panels reinforced by GPLs supporting on Winkler elastic foundation, Mech. Base. Des. Struct. Mach. 52 (6) (2024) 3552–3581.
[20] M. Babaei, et al., Stress wave propagation and natural frequency analysis of functionally graded graphene platelet-reinforced porous joined conical–cylindrical–conical shell, Waves Random Complex Media (2021) 1–33.
[21] M. Babaei, et al., Transient thermal stresses in FG porous rotating truncated cones reinforced by graphene platelets, Appl. Sci. 12 (8) (2022) 3932.
[22] M. Babaei, K. Asemi, Stress analysis of functionally graded saturated porous rotating thick truncated cone, Mech. Base. Des. Struct. Mach. 50 (5) (2022) 1537–1564.
[23] K. Asemi, M. Salehi, M. Akhlaghi, Transient thermal stresses in functionally graded thick truncated cones by graded finite element method, Int. J. Pres. Ves. Pip. 119 (2014) 52–61.
[24] K. Asemi, et al., Analysis of functionally graded thick truncated cone with finite length under hydrostatic internal pressure, Arch. Appl. Mech. 81 (2011) 1063–1074.
[25] K. Asemi, M. Salehi, M. Akhlaghi, Dynamic analysis of a functionally graded thick truncated cone with finite length, Int. J. Mech. Mater. Des. 6 (2010) 367–378.
[26] I. Pakravan, et al., Haar wavelet technique applied on the functionally graded carbon nanotube reinforced conical shells to study free vibration and buckling behaviors in thermal environments. Journal of Vibration and Control 28 (15–16) (2022) 1863–1878.
[27] C. Feng, H. Wu, X. Li, Buckling analysis of corroded pipelines under combined axial force and external pressure, Metals 12 (2) (2022) 308.
[28] A. Rudawska, The impact of the acidic environment on the mechanical properties of epoxy compounds in different conditions, Polymers 12 (12) (2020) 2957.
[29] S. Emam, M. Eltaher, Buckling and postbuckling of composite beams in hygrothermal environments, Compos. Struct. 152 (2016) 665–675.
[30] M. Biswal, S. Sahu, A. Asha, Experimental and numerical studies on free vibration of laminated composite shallow shells in hygrothermal environment, Compos. Struct. 127 (2015) 165–174.
[31] X. Song, et al., Vibration evolution of laminated composite conical shell with arbitrary foundation in hygrothermal environment: experimental and theoretical investigation, Mech. Syst. Signal Process. 200 (2023) 110565.
[32] M. Biswal, et al., Hygrothermal effects on buckling of composite shell-experimental and FEM results, Steel Compos. Struct. 22 (6) (2016) 1445–1463.
[33] A. Heidari-Soureshjani, et al., Hygrothermal vibro-buckling of FG ceramic-steel porous consolidated conical-conical shells, Thin-Walled Struct. 201 (2024) 112002.
[34] H. Dadras, et al., Indentation, finite element modeling and artificial neural network studies on mechanical behavior of GFRP composites in an acidic environment, J. Mater. Res. Technol. 24 (2023) 5042–5058.
[35] A. Seyfi, et al., Dispersion of elastic waves in functionally graded CNTs-reinforced composite beams, Appl. Sci. 12 (8) (2022) 3852.
[36] Kamarian, S., et al., Machine Learning for Bending Behavior of Sandwich Beams with 3D-Printed Core and Natural Fiber-Reinforced Composite Face Sheets. Polymer Composites.
[37] S. Vafaei, et al., Forced convection nanofluid heat transfer as a function of distance in microchannels, Materials 14 (11) (2021) 3021.
[38] J. Sunny, et al., Accelerated zero-stress hydrothermal aging of dry E-glass fibers and service life prediction using Arrhenius model, Fibers 11 (8) (2023) 70.
[39] M. Ayatollahi, R. Barbaz Isfahani, R. Moghimi Monfared, Effects of multi-walled carbon nanotube and nanosilica on tensile properties of woven carbon fabric-reinforced epoxy composites fabricated using VARIM, J. Compos. Mater. 51 (30) (2017) 4177–4188.
[40] B.A. Nayak, R.K. Prusty, B.C. Ray, Effect of nanosilica and nanoclay reinforcement on flexural and thermal properties of glass fiber/epoxy composites, Mater. Today: Proc. 33 (2020) 5098–5102.
[41] L.Y. Chen, et al., Enhanced thermal and mechanical properties of epoxy composites by spherical silica with different size, in: Key Eng. Mater 22, Trans Tech Publ, 2017, pp. 7–12.
[42] D. Kodali, et al., Mechanical and thermal properties of modified Georgian and Brazilian clay infused biobased epoxy nanocomposites, Mater. Chem. Phys. 257 (2021) 123821.
[43] V. Mahesh, Effect of alkaline environment on the properties of nanoclay/vinylester/glass nanocomposites, Int. J. Sci. Res. 1 (1) (2012) 6–11.
[44] Y. Gitiara, et al., Low-velocity impact behavior of incorporated GFRP composites with nanoclay and nanosilica in a corrosive environment: experimental and numerical study, J. Compos. Mater. 55 (27) (2021) 3989–4010.
[45] M. Rafiee, et al., Buckling resistant graphene nanocomposites, Appl. Phys. Lett. 95 (22) (2009) 223103.
[46] Ö. Özbek, Axial and lateral buckling analysis of kevlar/epoxy fiber-reinforced composite laminates incorporating silica nanoparticles, Polym. Compos. 42 (3) (2021) 1109–1122.

[47] Ö.Y. Bozkurt, et al., Axial and lateral buckling analysis of fiber reinforced S-glass/epoxy composites containing nano-clay particles, Compos. B Eng. 158 (2019) 82–91.
[48] C. Shu, H. Du, Implementation of clamped and simply supported boundary conditions in the GDQ free vibration analysis of beams and plates, Int. J. Solid Struct. 34 (7) (1997) 819–835.
[49] A. Talezadehlari, Free vibration analysis of perforated composite cylindrical shell and panel using multi-domain generalized differential quadrature (GDQ) method, Compos. Struct. 287 (2022) 115337.
[50] Q. Huang, et al., Free vibration analysis of carbon-fiber plain woven reinforced composite conical-cylindrical shell under thermal environment with general boundary conditions, Compos. Struct. 322 (2023) 117340.
[51] Q. You, et al., Efficient Analysis on Buckling of FG-CNT Reinforced Composite Joined Conical–Cylindrical Laminated Shells Based on GDQ Method under Multiple Loading Conditions. Mechanics of Advanced Materials and Structures, 2024, pp. 1–18.
[52] W.-M. Qian, et al., Investigation on the effect of functionalization of single-walled carbon nanotubes on the mechanical properties of epoxy glass composites: experimental and molecular dynamics simulation, J. Mater. Res. Technol. 12 (2021) 1931–1945.
[53] Y. Padarthi, et al., Assessment of transport kinetics and chemo-mechanical properties of GF/Epoxy composite under long term exposure to sulphuric acid, Polym. Degrad. Stabil. 183 (2021) 109436.
[54] M. Jawaid, A. Qaiss, R. Bouhfid, Nanoclay reinforced polymer composites 5 (2016) 23–29.
[55] P. Dittanet, R.A. Pearson, Effect of silica nanoparticle size on toughening mechanisms of filled epoxy, Polymer 53 (9) (2012) 1890–1905.
[56] L.Y. Chen, et al., Enhanced thermal and mechanical properties of epoxy composites by spherical silica with different size, Key Eng. Mater. 727 (2017) 519–526.
[57] K. Shaker, et al., Effect of silica particle loading on shape distortion in glass/vinyl ester-laminated composite plates, J. Text. Inst. 109 (5) (2018) 656–664.
[58] Hminghlui, L., et al., Experimental and Numerical Studies on the Mechanical Characteristics of Timoho Fiber Epoxy Composites with Nanofiller Addition. Polymer Composites.
[59] S. Mamallan, V. Narayanan, Demystifying the role of graphene nanoplatelets percentage and sonication duration on the mechanical properties of the glass fabric/graphene nanoplatelets hybrid nano-composite, Polym. Compos. 43 (11) (2022) 8170–8180.
[60] R. Barbaz-Isfahani, et al., A comprehensive investigation of the low-velocity impact response of enhanced GFRP composites with single and hybrid loading of various types of nanoparticles, Heliyon 9 (5) (2023) e15930.
[61] H. Panda, S. Sahu, P. Parhi, Hygrothermal effects on free vibration of delaminated woven fiber composite plates–Numerical and experimental results, Compos. Struct. 96 (2013) 502–513.
[62] G. Romeo, et al., *A New Test Facility for Measuring the Coefficient of Moisture Expansion of Advanced Composite Materials.* N97-717Z, 1991, p. 181.
[63] J. Abot, A. Yasmin, I. Daniel, Hygroscopic behavior of woven fabric carbon-epoxy composites, J. Reinforc. Plast. Compos. 24 (2) (2005) 195–207.
[64] H. Kang, D.S. Kim, A study on the crystallization and melting of PLA nanocomposites with cellulose nanocrystals by DSC, Polym. Compos. 44 (11) (2023) 7727–7736.
[65] M.R. Eslami, J. Eslami, M. Jacobs, Buckling and Postbuckling of Beams, Plates, and Shells, Springer, 2018.
[66] M. Mirzaei, Y. Kiani, Thermal buckling of temperature dependent FG-CNT reinforced composite conical shells. Aerospace Science and Technology 47 (2015) 42–53.
[67] J.N. Reddy, Mechanics of Laminated Composite Plates and Shells: Theory and Analysis, CRC press, 2003.
[68] A.K. Kaw, Mechanics of Composite Materials, CRC press, 2005.
[69] S. Kamarian, et al., Free vibration analysis of conical shells reinforced with agglomerated Carbon Nanotubes, Int. J. Mech. Sci. 108 (2016) 157–165.
[70] Y. Kiani, Buckling of functionally graded graphene reinforced conical shells under external pressure in thermal environment, Compos. B Eng. 156 (2019) 128–137.
[71] M. Akbari, Y. Kiani, M. Eslami, Thermal buckling of temperature-dependent FGM conical shells with arbitrary edge supports, Acta Mech. 226 (3) (2015) 897–915.
[72] G.J. Turvey, I.H. Marshall, Buckling and Postbuckling of Composite Plates, Springer Science & Business Media, 1994.
[73] X. Xiang, et al., A numerical solution for vibration analysis of composite laminated conical, cylindrical shell and annular plate structures. Composite Structures 111 (2014) 20–30.
[74] M. Alinia, et al., The effect of auxeticity on the vibration of conical sandwich shells with ring support under various boundary conditions. Engineering Analysis with Boundary Elements 152 (2023) 130–147.
[75] A. Heidari-Soureshjani, R. Talebitooti, M. Talebitooti, On the frequency characteristics of rotating combined conical-conical shells made of FG-CNTRC composite materials under thermal environments. Mechanics Based Design of Structures and Machines 52 (3) (2024) 1437–1461.
[76] S. Kamarian, et al., Influence of carbon nanotubes on thermal expansion coefficient and thermal buckling of polymer composite plates: experimental and numerical investigations. Mechanics Based Design of Structures and Machines 49 (2) (2021) 217–232.
[77] C. Shu, Differential Quadrature and its Application in Engineering, Springer Science & Business Media, 2012.
[78] A.A. Jahangiri, Y. Rostamiyan, Mechanical properties of nano-silica and nano-clay composites of phenol formaldehyde short carbon fibers, J. Compos. Mater. 54 (10) (2020) 1339–1352.
[79] S. Astaraki, et al., Determination of mechanical properties of nanocomposites reinforced with spherical silica nanoparticles using experiments, micromechanical model and finite elements method, J. Compos. Mater. 57 (17) (2023) 2689–2702.
[80] A.E. Krauklis, et al., Dissolution kinetics of R-glass fibres: influence of water acidity, temperature, and stress corrosion, Fibers 7 (3) (2019) 22.
[81] B. Wei, S. Song, H. Cao, Strengthening of basalt fibers with nano-SiO2–epoxy composite coating, Mater. Des. 32 (8–9) (2011) 4180–4186.
[82] S.M. Hosseini Farrash, J. Rezaeepazhand, M. Shariati, Experimental study on amine-functionalized carbon nanotubes' effect on the thermomechanical properties of CNT/epoxy nano-composites. Mechanics of advanced composite Structures 5 (1) (2018) 41–48.
[83] B. Singh, J.B. Babu, Thermal buckling of laminated conical shells embedded with and without piezoelectric layer, J. Reinforc. Plast. Compos. 28 (7) (2009) 791–812.
[84] B. Patel, K. Shukla, Y. Nath, Thermal postbuckling analysis of laminated cross-ply truncated circular conical shells, Compos. Struct. 71 (1) (2005) 101–114.
[85] R.K. Bhangale, N. Ganesan, C. Padmanabhan, Linear thermoelastic buckling and free vibration behavior of functionally graded truncated conical shells, J. Sound Vib. 292 (1–2) (2006) 341–371.